Faraday Discussions

Cite this: DOI: 10.1039/c7fd00145b

PAPER

Linking classical and molecular optomechanics descriptions of SERS

Mikołaj K. Schmidt,[abcd] Ruben Esteban,[ce] Felix Benz,[f] Jeremy J. Baumberg[f] and Javier Aizpurua *[ac]

Received 25th April 2017, Accepted 1st June 2017
DOI: 10.1039/c7fd00145b

The surface-enhanced Raman scattering (SERS) of molecular species in plasmonic cavities can be described as an optomechanical process where plasmons constitute an optical cavity of reduced effective mode volume which effectively couples to the vibrations of the molecules. An optomechanical Hamiltonian can address the full quantum dynamics of the system, including the phonon population build-up, the vibrational pumping regime, and the Stokes–anti-Stokes correlations of the photons emitted. Here we describe in detail two different levels of approximation to the methodological solution of the optomechanical Hamiltonian of a generic SERS configuration, and compare the results of each model in light of recent experiments. Furthermore, a phenomenological semi-classical approach based on a rate equation of the phonon population is demonstrated to be formally equivalent to that obtained from the full quantum optomechanical approach. The evolution of the Raman signal with laser intensity (thermal, vibrational pumping and instability regimes) is accurately addressed when this phenomenological semi-classical approach is properly extended to account for the anti-Stokes process. The formal equivalence between semi-classical and molecular optomechanics descriptions allows us to describe the vibrational pumping regime of SERS through the classical cross sections which characterize a nanosystem, thus setting a roadmap to describing molecular optomechanical effects in a variety of experimental situations.

1 Introduction

The Raman scattering of molecular species is an inelastic scattering process experienced by photons that illuminate a molecule or group of molecules, where

[a]Materials Physics Center CSIC-UPV/EHU, 20018 Donostia-San Sebastián, Spain. E-mail: aizpurua@ehu.eus
[b]Macquarie University Quantum Research Centre in Science and Technology (QSciTech), MQ Photonics Research Centre, Department of Physics and Astronomy, Macquarie University, NSW 2109, Australia. E-mail: mikolaj.schmidt@mq.edu.au
[c]Donostia International Physics Center DIPC, 20018 Donostia-San Sebastián, Spain
[d]Faculty of Physics, University of Warsaw, 02-093 Warsaw, Poland
[e]IKERBASQUE, Basque Foundation for Science, Maria Diaz de Haro 3, 48013 Bilbao, Spain
[f]NanoPhotonics Centre, Cavendish Laboratory, University of Cambridge, Cambridge, CB3 0HE, UK

the frequency of the scattered photons experiences a spectral shift that carries information on the vibrational structure of the molecule. In particular, incident photons with frequency ω_l can either lose or gain energy corresponding to the molecular phonon frequencies ω_m. These Stokes and anti-Stokes processes, respectively, induce excitation and relaxation between the rungs of the ladder of vibrational states of the molecule. In Surface-Enhanced Raman Scattering (SERS), the rates of these processes are strongly enhanced by placing the molecule near a metallic structure supporting surface plasmon resonances, which localize and enhance the electromagnetic local fields driving the inelastic processes at the molecule.

The SERS enhancement can also benefit from chemical effects due to electron transfer processes between the metal and the molecule, but the most important contribution is generally agreed to be electromagnetic in origin. In the simplest model, the presence of a plasmonic particle enhances both the intensity of the light exciting the molecule (photons in) and the emission rate (photons out) of the molecule. The increase of the Raman signal is thus approximately determined by the fourth power of the plasmonic enhancement of the local electric field at the position of the molecule, K, leading to SERS enhancement factors as large as $|K|^4 \sim 10^8$–10^{12}, under typical conditions in SERS supported by plasmonic nano-antennas, as for instance in plasmonic gaps.[1–4]

This simple description is particularly appropriate when the ladder of vibrational states of the molecule is populated predominantly through direct heating by the environment. However, if the intensity of the incident illumination is sufficiently increased, vibrational pumping of phonons through Stokes transitions can occur, exceeding the thermal population and strongly modifying the expected Raman response. Vibrational pumping has also been discussed in the literature in the context of Stokes anti-Stokes (SaS) correlations.[5–7] Many of the characteristics of SERS can be understood through a simple model which combines the electromagnetic $|K|^4$ enhancement factor with the thermal and vibrational phonon pumping mechanisms, formulated about 20 years ago.[8] Throughout our discussion, we will refer to this description as the phenomenological semi-classical (PSC) picture of SERS.

On the other hand, it has recently been pointed out that SERS can also be considered as a molecular optomechanical system.[9,10] In this picture, the polarizability of the molecule and, consequently, its interaction with a nearby plasmonic cavity, is explicitly dependent on the internal vibrational state of the molecule. When the system is excited by a laser, this plasmon–phonon coupling can induce modifications in the transitions between the vibrational levels, leading to an enhancement of the Raman signal that depends on the particular properties of the coupling and the external illumination. An analogous process can be found in typical optomechanical cavities, where the resonant frequency of a photonic cavity is modified by the oscillations of one (macroscopic) part of the system (for example, vibrations of the mirrors forming a Fabry–Pérot cavity).[11] In the initial paper pointing to the analogy between conventional optomechanical systems and SERS, the quantum-mechanical equations governing its dynamics were solved through the classical solution of the Langevin equations. Throughout this discussion, we will be referring to this approach as classical molecular optomechanics or CMO. We compare this analysis with a rigorous quantum treatment of the optomechanical Hamiltonian describing SERS (quantum MO or

QMO), which allows us to study effects such as photon correlations that cannot be generally treated by classical approaches.[5]

In this contribution, we discuss the differences and similarities between the descriptions of SERS offered by these three models (PSC, CMO and QMO). First, in Sections 2 and 3 we briefly introduce the three models, first developing the common framework of optomechanics for both the quantum as well as the classical approaches, and finally introducing the phenomenological semiclassical model in connection with the former two. For simplicity, we focus on the often-studied case of a point-like molecule characterized by a single vibrational mode along an arbitrary normal coordinate, described by a scalar Raman polarizability. Furthermore, we assume that the optical response of the plasmonic structure is characterized by a single Lorentzian-like cavity mode. The extension of the optomechanical model to more complex plasmonic structures and responses, showing an arbitrary number of quasi-normal modes, has been recently discussed.[12] In Section 2.4 we compare the results of classical and quantum optomechanical models (CMO and QMO), and in Section 3.1 we demonstrate that in the typical regimes of interaction explored in SERS experiments, a modified version of the PSC description of the Raman signals can yield results consistent with those obtained from the application of the full QMO. After a short outlook into the possible extensions of the optomechanical SERS models, emphasizing the outcome of non-classical predictions, in Section 4, we provide a brief discussion of the relationships between the three models and the conclusions.

2 Molecular optomechanics

We introduce in this section the optomechanical Hamiltonian commonly used to address the dynamics of a system where photons of an optical cavity and vibrations of a mechanical resonator are coupled. This theoretical framework will be applied to address molecular vibrations in a plasmonic nanocavity, by using two different methodological approaches to solve the optomechanical dynamics: a quantum molecular optomechanics (QMO) methodology as well as a classical molecular optomechanics (CMO) approach will be explicitly described, and the results obtained with each approach will be compared in typical situations of plasmon-induced vibrational molecular spectroscopy.

2.1 Introduction to molecular optomechanics

In the molecular optomechanical description of SERS, the interaction between the molecular vibrations and the photons in the plasmonic cavity is described by the interaction Hamiltonian[10]

$$H_{\mathrm{I}} = -\frac{1}{2}\hat{\mathbf{p}}(t)\cdot\hat{\mathbf{E}}(\mathbf{r}_{\mathrm{m}}, t), \tag{1}$$

where $\hat{\mathbf{p}}(t)$ and $\hat{\mathbf{E}}(\mathbf{r}_{\mathrm{m}},t)$ are the time-dependent operators of the quantized molecular polarization and electric fields, respectively, the latter evaluated at the molecule's position $\mathbf{r}_{\mathrm{m}}$. We note that this formula differs from that listed in our previous contributions,[10,13] as it includes a factor of 1/2. We consider this correction due to the fact that the Raman dipole used here is not permanent, but rather induced by the electric field of the plasmonic cavity (see *e.g.* the discussion in Chapter 8.1 of ref. 14). As we will see in Section 3.1, the quantum phonon

population obtained with the use of this expression reproduces the semi-classical phonon population. For a localized plasmonic resonance with a Lorentzian-like spectral response centered at ω_c and effective volume V, the electromagnetic fields at position $\mathbf{r}$ can be expressed as[15,16]

$$\hat{\mathbf{E}}(\mathbf{r},t) = \mathbf{u}_E\sqrt{\frac{\hbar\omega_c}{2V\varepsilon_0\varepsilon}}\left[\hat{a}(t)u(\mathbf{r}) + \hat{a}^\dagger(t)u^*(\mathbf{r})\right], \quad (2)$$

where $\hat{a}$ and $\hat{a}^\dagger$ are the bosonic annihilation and creation operators of the cavity excitations, or plasmons, oscillating at ω_c and $-\omega_c$, respectively, and $\mathbf{u}_E$ is a unit vector indicating the polarization. $\varepsilon_0\varepsilon$ is the permittivity of the surrounding medium and $u(\mathbf{r})$ gives the spatial variation of the electric fields, with $|u(\mathbf{r})| = 1$ at the point of maximum field strength.

On the other hand, the molecular polarization $\hat{\mathbf{p}}(t)$ is also induced by the electric field $\hat{\mathbf{E}}(\mathbf{r}_m,t)$ according to

$$\hat{\mathbf{p}}(t) = (L_m)^{1/4}\alpha_L(Q_k)\hat{\mathbf{E}}(\mathbf{r}_m,t). \quad (3)$$

Here $\alpha_L(Q_k)$ is the polarizability of the molecule, and depends on the normal mode coordinate Q_k, which, in the one-dimensional model used throughout this work, corresponds to the physical displacement of atoms in the molecule. The electromagnetic local field correction $(L_m)^{1/4} = (\varepsilon + 2)/3$ is included to account for the difference between the applied electric field and the local field inducing the Raman dipole.[17] For simplicity, throughout the paper we will use $\varepsilon = L_m = 1$. The polarizability can be expanded around the equilibrium configuration $Q_k = 0$ as

$$\alpha_L(Q_k) = \alpha_L(0) + \left(\frac{\partial\alpha_L}{\partial Q_k}\right)_{Q_k=0}Q_k + \ldots, \quad (4)$$

The term $\alpha_L(0)$ describes elastic excitation of the molecular vibrations, and here is considered to be zero. The second term in eqn (4) describes the Raman scattering, and is a function of the isotropic Raman tensor element $R_k = (\partial\alpha_L/\partial Q_k)_{Q_k=0}$ and the zero-point amplitude of the vibrations $Q_k^0 = \sqrt{\hbar/(2\omega_m)}$. Note that here we neglect any polarization effects associated with the depolarization of the scattered light.[17,18]

In the one-dimensional model, the potential landscape of the ground electronic state of the molecule plotted against Q_k (solid line in Fig. 1(a)) can be approximated as a displaced harmonic potential (dashed line in Fig. 1(a)). Therefore, the vibrational levels separated by phonon frequency ω_m (ref. 17 and 19) can be quantized using the phonon creation and annihilation operators $\hat{b}$ and $\hat{b}^\dagger$:

$$\hat{Q}_k = Q_k^0(\hat{b} + \hat{b}^\dagger). \quad (5)$$

We then obtain the interaction Hamiltonian

$$\hat{H}_I(t) = -Q_k^0R_k\frac{\hbar\omega_c}{4\varepsilon_0\varepsilon V}\left(\hat{b} + \hat{b}^\dagger\right)\left[\hat{a}(t)u(\mathbf{r}_m) + \hat{a}^\dagger(t)u^*(\mathbf{r}_m)\right]^2(\mathbf{u}_E\cdot\mathbf{u}_k)^2. \quad (6)$$

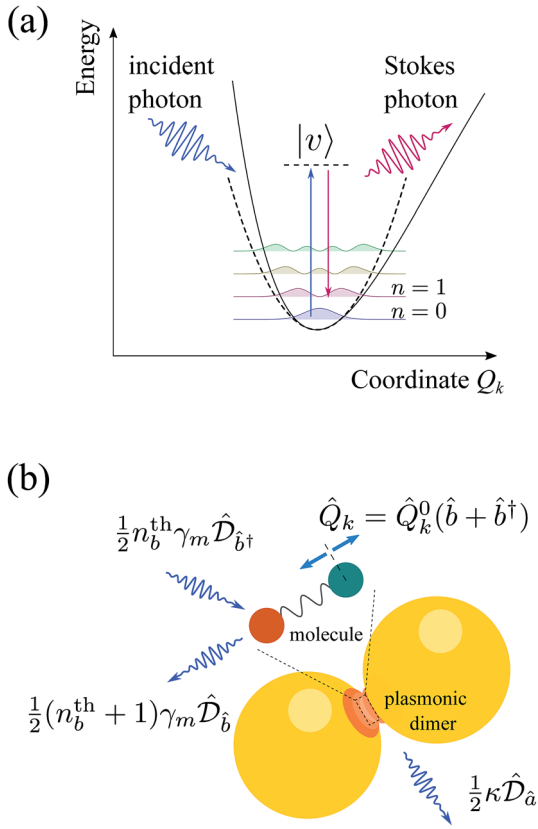

Fig. 1 (a) Energy landscape of the ground electronic state of a molecule (solid line) along the atomic coordinate Q_k approximated by a harmonic potential (dashed line). The two-photon Raman transitions between vibrational levels through the virtual state $|v\rangle$ are marked with solid arrows. (b) Schematic of a typical single-molecule SERS setup, with the molecule positioned in the gap of a plasmonic dimer antenna. Decay and thermal pumping processes leading to transitions between the states of the vibrations ($\mathscr{D}_{\hat{b}}$, $\mathscr{D}_{\hat{b}^\dagger}$) and decay of the plasmonic cavity ($\mathscr{D}_{\hat{a}}$) are described with the respective Lindblad–Kossakowski terms in the master equation (eqn (11)).

In the expansion of the last equation (square brackets) we neglect the two terms oscillating at $\pm 2\omega_c$ frequencies, as those will not play a role in the interaction. The remaining two terms can be rewritten using the boson commutation rules as

$$\hat{a}^\dagger\hat{a} + \hat{a}\hat{a}^\dagger = 2\hat{a}^\dagger\hat{a} + 1. \tag{7}$$

The last term does not contribute to the coupling of the cavity with vibrations, and can be considered as a static displacement of the equilibrium position of the vibrations $\hat{Q}_k \propto (\hat{b} + \hat{b}^\dagger)$ which does not play a role in the dynamics of the system.

The complete Hamiltonian also includes the expression for the energies of the cavity excitation ($\hbar\omega_c$) and phonons ($\hbar\omega_m$). Furthermore, we include the coherent excitation by the laser with frequency ω_l and pumping rate Ω (see Appendix B for

a detailed discussion of the relationship between Ω and the laser intensity I_l). Eventually we obtain:

$$\hat{H} = \hbar\omega_m \hat{b}^\dagger \hat{b} + \hbar\omega_c \hat{a}^\dagger \hat{a} - \hbar g_0 \hat{a}^\dagger \hat{a}(\hat{b}^\dagger + \hat{b}) + i\hbar\Omega(\hat{a}^\dagger e^{-i\omega_l t} - \hat{a}e^{i\omega_l t}) \quad (8)$$

where g_0 is the single-plasmon optomechanical coupling rate

$$g_0 = \frac{Q_k^0 R_k \omega_c}{2\varepsilon_0 \varepsilon V} |u(\mathbf{r}_m)|^2 (\mathbf{u}_E \cdot \mathbf{u}_k)^2. \quad (9)$$

By placing the molecule in the hottest spot of the quasi-mode where $|u(\mathbf{r}_m)|^2 = 1$, and assuming the direction of oscillation is parallel to the fields at this point $\mathbf{u}_E \cdot \mathbf{u}_k = 1$, we can maximize the coupling:

$$g_0 = \frac{Q_k^0 R_k \omega_c}{2\varepsilon_0 \varepsilon V}. \quad (10)$$

We note that a similar Hamiltonian for Raman scattering, in which the incident and inelastically scattered photons are described as excitations of two different modes, was recently proposed by Parra-Murillo *et al.*[6]

To complete the description or our model, we need to consider the interaction of the plasmons and the vibrations with the environment. These incoherent effects are included by considering the master equation for the evolution of the density matrix of the system:

$$\partial_t \rho = \frac{i}{\hbar}[\rho, \hat{H}] + \frac{\kappa}{2}\mathscr{D}_{\hat{a}}[\rho] + \frac{(n_b^{th}+1)\gamma_m}{2} D_{\hat{b}}[\rho] + \frac{n_b^{th}\gamma_m}{2} D_{\hat{b}^\dagger}[\rho]. \quad (11)$$

The first term after the commutator describes the decay of the plasmons (κ is the decay rate of the plasmon), and is proportional to the Lindblad–Kossakowski superoperator $\mathscr{D}_{\hat{a}}[\rho]$, where[20,21]

$$\mathscr{D}_{\hat{O}}[\rho] = 2\hat{O}\rho\hat{O}^\dagger - \hat{O}^\dagger\hat{O}\rho - \rho\hat{O}^\dagger\hat{O}. \quad (12)$$

The decay and incoherent pumping of the mechanical vibrations by thermal excitations in the environment at temperature T are described by the last two terms in eqn (11), with γ_m as the decay rate of the molecular vibration and $n_b^{th} = (e^{\hbar\omega_m/k_B T} - 1)^{-1}$ as the thermal population of vibrations where k_B is the Boltzmann constant.

2.2 Quantum-mechanical approach to molecular optomechanics (QMO)

If the interaction between the plasmonic and vibrational degrees of freedom is weak ($g_0 \ll \kappa$), the coherently pumped cavity will remain very close to the coherent state α, with only small fluctuations around it denoted by δa ($\hat{a} \rightarrow \alpha + \delta\hat{a}$). Consequently, the vibrational degree of freedom is coherently pumped by the plasmon and the phonon operators can be represented as fluctuations $\delta\hat{b}$ around the coherent amplitude β ($\hat{b} \rightarrow \beta + \delta\hat{b}$). Amplitudes α and β, derived in Appendix A, take the form

$$\alpha = \frac{\Omega}{\kappa/2 + \mathrm{i}[\Delta - 2g_0\mathrm{Re}(\beta)]}, \quad \beta = \frac{g_0|\alpha|^2}{\omega_\mathrm{m} - \mathrm{i}\gamma_\mathrm{m}/2}, \tag{13}$$

where $\Delta = \omega_\mathrm{c} - \omega_\mathrm{l}$. We can also impose an arbitrary phase on the cavity fluctuation operator – for convenience we choose $\delta\hat{a} \rightarrow \delta\hat{a}\, \mathrm{e}^{\mathrm{i}\ \arg(\alpha)}$.

With these new operators $\delta\hat{a}$ and $\delta\hat{b}$, the optomechanical Hamiltonian in eqn (8) in the frame rotating with the frequency of incident illumination ω_l, can be rewritten as

$$\begin{aligned}\hat{H} = {} & \hbar\omega_\mathrm{m}\delta\hat{b}^\dagger\delta\hat{b} + \hbar\Delta'\delta\hat{a}^\dagger\delta\hat{a} - \hbar g_0|\alpha|(\delta\hat{a}^\dagger + \delta\hat{a})(\delta\hat{b}^\dagger + \delta\hat{b}) \\ & - \hbar g_0\delta\hat{a}^\dagger\delta\hat{a}(\delta\hat{b}^\dagger + \delta\hat{b}).\end{aligned} \tag{14}$$

The correction to the detuning $\Delta' - \Delta = -2g_0\mathrm{Re}(\beta) \approx -2{g_0}^2|\alpha|^2/\omega_\mathrm{m}$ is negligible in most optomechanical platforms, including typical SERS experiments. With the fluctuation $\delta\hat{a}$ very small compared with the coherent amplitude α, the last term in eqn (14) can usually be dropped, leading to the linearized optomechanical Hamiltonian $\hat{H}_\mathrm{lin}$:

$$\hat{H}_\mathrm{lin} = \hbar\omega_\mathrm{m}\delta\hat{b}^\dagger\delta\hat{b} + \hbar\Delta'\delta\hat{a}^\dagger\delta\hat{a} - \hbar g(\delta\hat{a}^\dagger + \delta\hat{a})(\delta\hat{b}^\dagger + \delta\hat{b}), \tag{15}$$

with $g = |\alpha|g_0$ being the effective optomechanical coupling proportional to the coherent pumping rate Ω. In this formulation, with the definitions in eqn (13), the expectation values of the fluctuations in the steady state (denoted by $\langle\ldots\rangle_\mathrm{ss}$) will vanish

$$\langle\delta\hat{a}\rangle_\mathrm{ss} = \langle\delta\hat{b}\rangle_\mathrm{ss} = 0. \tag{16}$$

The common approach to solving the optomechanical Hamiltonian in the weak-coupling regime ($g \ll \kappa$) relies on considering the optical cavity as a structured bath of excitations coupled to the vibrational structure of interest.[22,23] Mathematically, this translates into introducing the reduced density matrix of the vibrational subsystem ρ_b obtained by tracing out the optical degrees of freedom and solving the corresponding master equation:[24]

$$\begin{aligned}\frac{\mathrm{d}}{\mathrm{d}t}\rho_\mathrm{b} = {} & -\mathrm{i}\left[(\omega_\mathrm{m} + \Delta_\mathrm{m})\delta\hat{b}^\dagger\delta\hat{b},\ \rho_\mathrm{b}\right] + \frac{1}{2}\{\gamma_\mathrm{m}[n_\mathrm{th} + 1] + \Gamma_-\}\mathscr{D}_{\delta\hat{b}}(\rho_\mathrm{b}) \\ & + \frac{1}{2}[\gamma_\mathrm{m}n_\mathrm{th} + \Gamma_+]\mathscr{D}_{\delta\hat{b}^\dagger}(\rho_\mathrm{b}).\end{aligned} \tag{17}$$

The renormalization of the phonon energy Δ_m, reminiscent of the analogue Lamb shift in resonant systems, is due to the optical spring effect[11] and is negligible in typical molecular optomechanics systems (see eqn (74) later in the text). In this picture the role of the optical cavity is limited to modifying the transition rates between vibrational states $\Gamma_\pm$, which describe the creation

$$\Gamma_+ = \frac{{g_0}^2|\alpha|^2\kappa}{\left(\Delta' + \omega_\mathrm{m}\right)^2 + \left(\kappa/2\right)^2} \tag{18}$$

and annihilation

$$\Gamma_- = \frac{{g_0}^2|\alpha|^2\kappa}{(\Delta' - \omega_m)^2 + (\kappa/2)^2} \tag{19}$$

of phonons. In Fig. 2(a) we plot the transition rates, Γ_+ and Γ_-, for a typical plasmonic cavity where $\omega_m \sim \kappa$, with the laser blue-detuned from the cavity resonance ($\Delta = \omega_c - \omega_l < 0$). The cavity promotes the Stokes transitions ($\Gamma_- < \Gamma_+$) which pump phonons into the molecule, leading to the amplification of phonon population. In the opposite regime of red-detuned laser, illustrated in Fig. 2(b), the cavity promotes anti-Stokes transitions which remove phonons from the molecule, leading to the cooling of vibrations.

Significantly, this interpretation opens a pathway to describing the optomechanical response of a molecule positioned in an optical cavity system characterized by an arbitrary spectral density, which yields transition rates in the form of continuous functions of Stokes and anti-Stokes emission wavelengths, $\Gamma_\pm = \Gamma(\omega_l \mp \omega_m)$. Such a generalization has been recently proposed by Dezfouli and Hughes.[12]

2.2.1 Rate equations in QMO. To discuss the effect of the modification of transition rates systematically, we can derive from the master equation of the vibrational subsystem (eqn (17)), the rate equation for the incoherent phonon population, defined by the displaced operators $n_{\delta b} = \langle \delta\hat{b}^\dagger \delta\hat{b}\rangle_{ss}$:

$$\frac{dn_{\delta b}}{dt} = -n_{\delta b}(\gamma_m + \Gamma_-) + (n_{\delta b} + 1)\Gamma_+ + \gamma_m n_b^{th}. \tag{20}$$

This form yields a very intuitive picture of the system's dynamics. The expression in the first brackets describes the population decay through spontaneous emission ($\gamma_m n_{\delta b}$) and due to anti-Stokes emission ($\Gamma_- n_{\delta b}$). The second term captures the pumping of vibrational states by to Stokes processes, with $\Gamma_+ n_{\delta b}$ describing stimulated excitation. The last term in eqn (20) describes the balance between absorption and emission of phonons from and to the thermal bath, respectively.

The steady stated population of phonons is then

$$n_{\delta b} = \frac{\gamma_m}{\gamma_m + \Gamma_{opt}} n_b^{th} + \frac{\Gamma_+}{\gamma_m + \Gamma_{opt}}, \tag{21}$$

where

$$\begin{aligned}\Gamma_{opt} &= \Gamma_- - \Gamma_+ \\ &= {g_0}^2|\alpha|^2\kappa\left[\frac{1}{(\Delta' - \omega_m)^2 + (\kappa/2)^2} - \frac{1}{(\Delta' + \omega_m)^2 + (\kappa/2)^2}\right],\end{aligned} \tag{22}$$

is the optomechanical damping. In Fig. 2(c) we plot the dependence of the optomechanical damping Γ_{opt}, normalized by the phonon decay γ_m as a function of the detuning Δ.

The negative value of the optomechanical damping Γ_{opt} found for the blue-detuned laser (sketch in Fig. 2(a)) and, equivalently, for the $\Delta < 0$ part of the spectrum of Γ_{opt} shown Fig. 2(c)), yields an amplification of the phonon population through the reduction of the effective damping rate $\Gamma_{opt} + \gamma_m < \gamma_m$. As we will discuss later in detail, the intensities of the Stokes and anti-Stokes processes

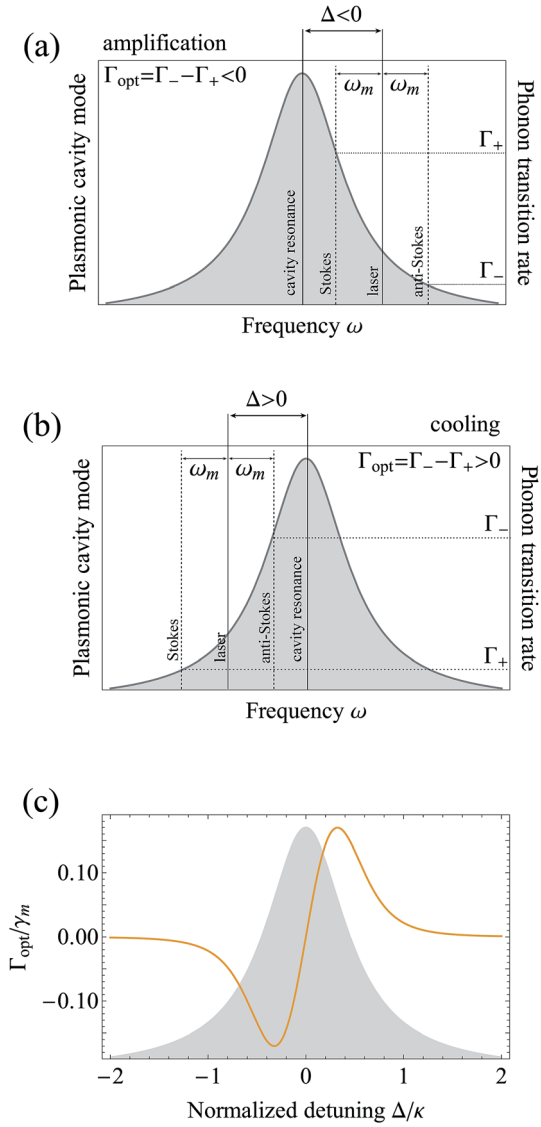

Fig. 2 Optomechanical damping parameter Γ_{opt} in the (a) amplification and (b) cooling setup. For the negative detuning (a) the Stokes emission rate Γ_+ determined by the amplitude of the plasmonic cavity mode at Stokes frequency $\omega_l - \omega_m$ dominates over the anti-Stokes rate Γ_-, calculated at anti-Stokes emission frequency $\omega_l + \omega_m$, yielding negative optomechanical damping Γ_{opt}. For positive detuning (b) $\Gamma_- > \Gamma_+$ the relationship is reversed, resulting in positive Γ_{opt}. (c) Normalized optomechanical damping Γ_{opt}/γ_m as a function of detuning Δ. The parameters are $\hbar g_0 = 10$ meV, $\hbar\Omega = 60$ meV, $\hbar\omega_m = 100$ meV, $\hbar\kappa = 250$ meV, $\hbar\gamma_m = 1$ meV.

are dependent on the phonon population. Consequently, the amplification of phonons through negative Γ_{opt} will result in increased Raman scattering intensities.

Conversely, the positive optomechanical damping found for $\Delta > 0$ (Fig. 2(b) and $\Delta > 0$ part of the spectrum in (c)) provides the basis for the sideband cooling

technique utilized in numerous optomechanical systems to reduce the population of vibrations below that provided by the thermal bath. In SERS, this effect will thus lead to the suppression of the anti-Stokes scattering intensity.

Additionally, we would like to pay attention to a situation little explored in standard optomechanics: the laser tuned to the cavity, $\Delta = 0$. In this case, the optomechanical damping rate Γ_{opt} vanishes due to the symmetry of the cavity profile, yet we still expect to observe the buildup of phonon populations due to the intrinsic asymmetry of the Stokes ($\propto \Gamma_{+}(n_{\delta\mathrm{b}} + 1)$) and anti-Stokes ($\propto \Gamma_{-} n_{\delta\mathrm{b}}$) terms. Indeed, in this limit of zero optomechanical damping, we obtain

$$\lim_{\Delta \to 0} n_{\delta\mathrm{b}} = n_{\mathrm{b}}^{\mathrm{th}} + \frac{4{g_0}^2|\alpha|^2}{\kappa^2 + 4{\omega_{\mathrm{m}}}^2} \frac{\kappa}{\gamma_{\mathrm{m}}}. \tag{23}$$

Last, we recall that the master equation of the dynamics of the vibrational subsystem (eqn (17)) is written with the displaced phonon operators $\hat{b} \to \beta + \delta\hat{b}$. The total phonon population, accounting for the coherent displacement amplitude β, is given by

$$n_{\mathrm{b}} = \left\langle \hat{b}^{\dagger} \hat{b} \right\rangle_{\mathrm{ss}} = \left\langle \left(\beta^* + \delta\hat{b}^{\dagger}\right)\left(\beta + \delta\hat{b}\right) \right\rangle_{\mathrm{ss}} = |\beta|^2 + \left\langle \delta\hat{b}^{\dagger} \delta\hat{b} \right\rangle_{\mathrm{ss}} = |\beta|^2 + n_{\delta\mathrm{b}}, \tag{24}$$

where we made use of the property of the displaced operators δb given by eqn (16). The coherent populations $|\beta|^2$ in typical MO system are usually negligible compared to the thermally or vibrationally pumped populations captured by $n_{\delta\mathrm{b}}$, so we can put $n_{\mathrm{b}} \approx n_{\delta\mathrm{b}}$. Throughout the rest of the discussion – in particular, when comparing the predictions of the QMO with semi-classical models – we will be referring to $n_{\delta\mathrm{b}}$ as the phonon population.

2.2.2 Emission spectra in QMO. While the information about the phonon population provides the details of the Raman processes, it is usually difficult to access experimentally. Therefore, studies of SERS are usually limited to measuring the inelastic scattering spectra and the intensities of the signals. We can calculate the emission spectra from the cavity as

$$S(\omega) = \omega^4 \int_{-\infty}^{\infty} \mathrm{d}t \mathrm{e}^{-\mathrm{i}\omega t} \left\langle \hat{a}^{\dagger}(t)\hat{a}(0) \right\rangle_{\mathrm{ss}}, \tag{25}$$

where the factor ω^4 is added to account for the characteristics of the dipolar emission. The two time correlations are calculated by inserting the solution of the master equation for the vibrational subsystem (eqn (17)) into the quantum Heisenberg–Langevin equations for $\hat{a}$ (this equation is derived in Appendix A and given explicitly in eqn (72)). In the weak coupling limit the cavity plasmon will decay before it can cascade down two vibrational states, and thus the inelastic part of the emission spectrum contains only the single-phonon scattering terms centered around $\omega_{\mathrm{l}} \pm \omega_{\mathrm{m}}$, with the linewidths of Stokes and anti-Stokes peaks modified by the optomechanical damping Γ_{opt}:[25]

$$\begin{aligned} S(\omega) \propto\ & n_{\delta\mathrm{b}} \omega^4 \Gamma_{-} \frac{\Gamma_{\mathrm{opt}} + \gamma_{\mathrm{m}}}{\left(\omega - \omega_{\mathrm{l}} - \omega_{\mathrm{m}}\right)^2 + \left(\Gamma_{\mathrm{opt}} + \gamma_{\mathrm{m}}\right)^2} \\ & + (n_{\delta\mathrm{b}} + 1)\omega^4 \Gamma_{+} \frac{\Gamma_{\mathrm{opt}} + \gamma_{\mathrm{m}}}{\left(\omega - \omega_{\mathrm{l}} + \omega_{\mathrm{m}}\right)^2 + \left(\Gamma_{\mathrm{opt}} + \gamma_{\mathrm{m}}\right)^2}. \end{aligned} \tag{26}$$

Thus, the peak intensities of the Stokes and anti-Stokes emission are given by

$$S(\omega_{aS}) \propto {\omega_{aS}}^4 \Gamma_- \frac{n_{\delta b}}{\Gamma_{opt} + \gamma_m}, \quad \text{and} \quad S(\omega_S) \propto {\omega_S}^4 \Gamma_+ \frac{n_{\delta b} + 1}{\Gamma_{opt} + \gamma_m}, \tag{27}$$

respectively. The intensities integrated over the widths of emission peaks are

$$\tilde{S}(\omega_{aS}) \propto {\omega_{aS}}^4 \Gamma_- n_{\delta b}, \quad \text{and} \quad \tilde{S}(\omega_S) \propto {\omega_S}^4 \Gamma_+ (n_{\delta b} + 1). \tag{28}$$

2.3 Classical theory of molecular optomechanics (CMO)

In the initial work connecting optomechanics and SERS,[9] the optomechanical Hamiltonian (eqn (8)) was solved using classical Langevin equations for the dynamics of the plasmonic and vibrational degrees of freedom. While this solution offered similar insights into the mechanism of the optomechanical heating and cooling of vibrations, as in the QMO model, it also provided different expressions for the population of phonons and scattering intensities. In this section we briefly present this formalism, which we dub classical molecular optomechanics or CMO.

As was the case within the QMO model, we begin by linearizing the optomechanical Hamiltonian given in eqn (8). However, in the current approach, we only displace the plasmon operator $\hat{a}$ by a coherent amplitude of the uncoupled cavity $\hat{a} \rightarrow \delta\hat{a} + \alpha^{(CMO)}$, with $\alpha^{(CMO)} = \Omega/(i\Delta + \kappa/2)$. As we did in the previous section for the QMO, we add a phase factor to $\delta\hat{a}$ and arrive at the linearized Hamiltonian:

$$\hat{H}_{lin}^{(CMO)} = \hbar\omega_m \hat{b}^\dagger \hat{b} + \hbar\Delta \delta\hat{a}^\dagger \delta\hat{a} - \hbar g^{(CMO)}(\delta\hat{a}^\dagger + \delta\hat{a})(\hat{b}^\dagger + \hat{b}) - \hbar g_0 |\alpha^{(CMO)}|^2 (\hat{b}^\dagger + \hat{b}), \tag{29}$$

with $g^{(CMO)} = g_0|\alpha^{(CMO)}|$. Importantly, this displacement of cavity operators does not guarantee the vanishing of the expectation values of $\delta\hat{a}$ nor that of $\hat{b}$, as was the case in the QMO (eqn (16)). However, since the differences between α and $\alpha^{(CMO)}$ are small in typical molecular optomechanical systems, we can consider $\alpha \approx \alpha^{(CMO)}$ and $g \approx g^{(CMO)}$.

The Heisenberg–Langevin equations derived from this Hamiltonian are:

$$\dot{\delta\hat{a}} = -(\kappa/2 + i\Delta)\delta\hat{a} + ig^{(CMO)}\left(\hat{b} + \hat{b}^\dagger\right) + \sqrt{\kappa}\hat{a}_{in}(t), \tag{30}$$

$$\dot{\hat{b}} = -(\gamma_m/2 + i\omega_m)\hat{b} + ig^{(CMO)}\left(\delta\hat{a} + \delta\hat{a}^\dagger\right) + ig_0|\alpha|^2 + \sqrt{\gamma_m}\hat{b}_{in}(t), \tag{31}$$

where the noise terms are:

$$\langle \hat{a}_{in}(t) \rangle = 0, \ \langle \hat{a}_{in}(t)\hat{a}_{in}^\dagger(t') \rangle = \delta(t - t'), \tag{32}$$

$$\langle \hat{b}_{in}(t) \rangle = 0, \ \langle \hat{b}_{in}^\dagger(t)\hat{b}_{in}(t') \rangle = n_b^{th}\delta(t - t'). \tag{33}$$

Notably, the thermal population is included in the model *via* eqn (33). To solve these equations, Roelli *et al.* considered a classical approximation by representing the cavity fluctuations as a sum of classical fields oscillating at the Stokes $(\Delta + \omega_m)$ and anti-Stokes $(\Delta - \omega_m)$ frequencies. Similarly, the mechanical oscillations were described as $\langle \hat{x}(t) \rangle \propto \langle \hat{b} + \hat{b}^\dagger \rangle \propto \cos(\omega_m t)$.[9,26]

2.3.1 Phonon population and emission spectrum. Eqn (30) and (31) can be solved in frequency space to provide the classical picture of the optomechanical damping Γ_{opt} and optical spring effects which modify the damping rate, and the natural frequency of the mechanical oscillator, respectively (see SI in ref. 9 for details and the complete derivation). The expressions for $\Gamma_{\pm} = {g_0}^2|\alpha^{(\mathrm{CMO})}|^2\kappa/[(\Delta \pm \omega_{\mathrm{m}})^2 + (\kappa/2)^2]$, and consequently Γ_{opt}, are very similar to those derived in the QMO, with the only difference being that $\alpha^{(\mathrm{CMO})}$ appears instead of α. In this framework, the phonon population $n_{\mathrm{b}}^{(\mathrm{CMO})}$ is proportional to the thermal population $n_{\mathrm{b}}^{\mathrm{th}}$, following:

$$n_{\mathrm{b}}^{(\mathrm{CMO})} = \frac{\gamma_{\mathrm{m}}}{\gamma_{\mathrm{m}} + \Gamma_{\mathrm{opt}}} n_{\mathrm{b}}^{\mathrm{th}}. \tag{34}$$

In analogy to the interpretation introduced for the QMO, we can see eqn (34) as a solution to a rate equation:

$$\frac{\mathrm{d}n_{\mathrm{b}}^{(\mathrm{CMO})}}{\mathrm{d}t} = -n_{\mathrm{b}}^{(\mathrm{CMO})}(\gamma_{\mathrm{m}} + \Gamma_{-} - \Gamma_{+}) + \gamma_{\mathrm{m}} n_{\mathrm{b}}^{\mathrm{th}}. \tag{35}$$

To calculate the emission spectrum, we can again solve the Heisenberg–Langevin equation for $\dot{\delta}\hat{a}$ (eqn (17)),[22,23,27] and arrive at

$$\begin{aligned} S^{(\mathrm{CMO})}(\omega) \propto\, & n_{\mathrm{b}}^{(\mathrm{CMO})}\omega^4\Gamma_{-}\frac{\Gamma_{\mathrm{opt}} + \gamma_{\mathrm{m}}}{(\omega - \omega_{\mathrm{l}} - \omega_{\mathrm{m}})^2 + \left(\Gamma_{\mathrm{opt}} + \gamma_{\mathrm{m}}\right)^2} \\ & + \left(n_{\mathrm{b}}^{(\mathrm{CMO})} + 1\right)\omega^4\Gamma_{+}\frac{\Gamma_{\mathrm{opt}} + \gamma_{\mathrm{m}}}{(\omega - \omega_{\mathrm{l}} + \omega_{\mathrm{m}})^2 + \left(\Gamma_{\mathrm{opt}} + \gamma_{\mathrm{m}}\right)^2}. \end{aligned} \tag{36}$$

After integrating the Raman peaks along the frequency of emission, the total power of the Stokes, $\tilde{S}^{(\mathrm{CMO})}(\omega_{\mathrm{S}})$, and anti-Stokes, $\tilde{S}^{(\mathrm{CMO})}(\omega_{\mathrm{aS}})$, signals can be derived in this classical framework as:

$$\tilde{S}^{(\mathrm{CMO})}(\omega_{\mathrm{aS}}) \propto {\omega_{\mathrm{aS}}}^4\Gamma_{-}n_{\mathrm{b}}^{(\mathrm{CMO})}, \tag{37}$$

$$\tilde{S}^{(\mathrm{CMO})}(\omega_{\mathrm{S}}) \propto {\omega_{\mathrm{S}}}^4\Gamma_{+}(n_{\mathrm{b}}^{(\mathrm{CMO})} + 1). \tag{38}$$

2.4 Comparison between classical and quantum molecular optomechanics

In this section, we compare the main characteristics and predictions of the two models presented in the previous sections, derived from a common optomechanical framework, and apply them to the context of Raman scattering in plasmonic cavities. Comparing the emission spectra from the QMO in eqn (26) and those from the CMO in eqn (36), we find that any difference between the two is a direct consequence of the contrasting expressions for the phonon populations (eqn (21) and (34)). Therefore, our discussion puts special emphasis on the different power dependencies of the phonon population as a function of the intensity of the excitation laser.

A first intuitive understanding of the differences arising from both approaches can be gained by looking at the corresponding rate equations for the phonon

populations (eqn (20) and (35)). The rate equations derived within the QMO (eqn (20)) and CMO (eqn (35)) models differ fundamentally in that the CMO appears not to include the direct pumping of populations through the Stokes transitions (the term describing the population-independent excitation rate Γ_+). We associate this term with the vibrational pumping.

Due to the difference quoted above, one can expect that a classical description based on the CMO will underestimate the population of phonons, and consequently will exhibit a weaker power dependence of emission on the incident laser intensity compared to that found within the QMO approach. We compare the phonon populations and emissions predicted by the two models as we increase the laser intensity, and relate these magnitudes to some measurements from previous experimental work. Indeed, the phonon populations discussed here can be extracted from SERS experiments by measuring the anti-Stokes to Stokes ratio. Here we particularly focus on the following properties of the thermal and vibrational pumping regimes of SERS:

• Linear dependency of the Stokes emission intensities on the power of the incident laser for both thermal and vibrational pumping regimes.

• Linear and quadratic dependency of the anti-Stokes intensity on the power of the incident laser for thermal and vibrational pumping regimes, respectively.

• Anti-Stokes to Stokes ratio exceeding that expected from an exclusively thermal distribution, for situations where the phonon population due to vibrational pumping dominates.

Additionally, we show that for sufficiently strong laser power, we can go beyond these simple dependencies due to two effects: (i) the onset of phonon-stimulated Raman transitions and (ii) parametric instability. While the latter process is described by both optomechanical models, the former, induced by the vibrational pumping of phonons, is only addressed by the QMO. In these regimes, the Stokes emission behaves non-linearly with the incident laser intensity.

2.4.1 Power dependence in QMO. Let us first consider the QMO model in the case of weak laser illumination and sufficiently low coupling strength g_0 and detuning Δ, so that the population $n_{\delta b} \ll 1$ and $|\Gamma_{opt}| \ll \gamma_m$. In this case,

$$n_{\delta b} \approx n_b^{th} + \frac{4{g_0}^2|\alpha|^2}{\kappa^2 + 4(\Delta' + \omega_m)^2}\frac{\kappa}{\gamma_m}, \tag{39}$$

indicating that the phonon population is the sum of the thermal population and a vibrational term proportional to $|\alpha|^2$ or, equivalently, to the laser intensity I_l ($I_l \propto |\alpha|^2$), see discussion in Appendix B. We illustrate this in Fig. 3(a), where we plot the phonon populations obtained within QMO as a function of the laser power I_l with blue lines. Solid and dashed blue lines correspond to the incident laser being blue-detuned ($\Delta = -\omega_m$) or resonant ($\Delta = 0$) to the cavity resonance, respectively. For the weakest pumping, the two lines overlap at the value $n_{\delta b} = n_b^{th}$, the characteristic phonon population of the thermal regime. Further increase of the illumination intensity leads to the onset of the vibrational pumping regime in which the phonon ladder is populated predominantly by the Stokes transitions, described by the second term in eqn (39), proportional to $|\alpha|^2$ (or equivalently, I_l).

In this illumination regime, the Stokes and anti-Stokes scattering given by eqn (27) exhibit the following intensity dependencies:

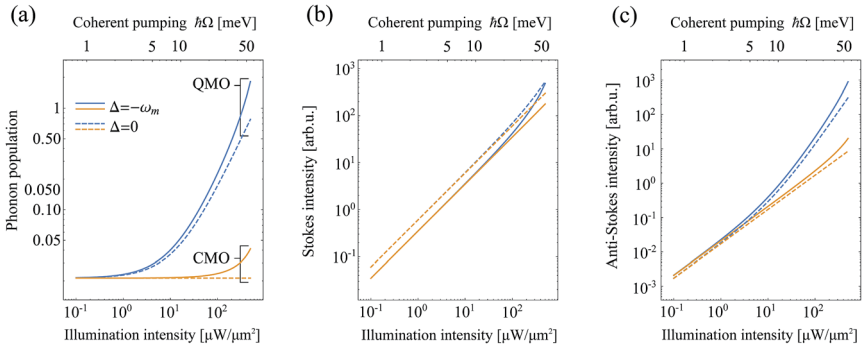

Fig. 3 Comparison of the phonon populations and Raman scattering intensities obtained from the two optomechanical models as a function of the illumination intensity I_l or coherent pumping Ω (see Appendix B). (a) Phonon populations $n_{\delta b}$ (blue lines) and $n_b^{(CMO)}$ (orange lines) for detunings $\Delta = -\omega_m = \kappa/2$ (solid lines) and $\Delta = 0$ (dashed lines). For the vanishing detuning case, the onset of parametric instability is not observed for the largest pumping intensities, and thus non-linearities originate from phonon-stimulated processes. (b) Stokes and (c) anti-Stokes emission intensities as obtained from the QMO theory (blue lines) and within the CMO approach (orange lines). The detunings are chosen and denoted as in (a). Thermal population $n_b^{th} = 0.02$, radiative yield $\eta = 0.5$, $\hbar g_0 = \hbar\kappa/12.5 = 20$ meV and $\hbar\omega_c = 2.5$ eV everywhere.

$$\begin{aligned} S(\omega_S) &\propto |\alpha|^2(1+n_{\delta b}) \propto I_l, \\ S(\omega_{aS}) &\propto |\alpha|^2 n_{\delta b} \propto I_l + \mathscr{C} I_l^2, \end{aligned} \tag{40}$$

where $\mathscr{C}$ is a parameter governing the relative contributions of the thermal and vibrational phonons to the signal (see eqn (39)). For weak illumination, the system remains in the thermal regime, and the anti-Stokes emission is proportional to the intensity I_l. For stronger illumination, we enter the vibrational pumping regime, and the anti-Stokes emission becomes quadratic with I_l. In contrast, the Stokes signal remains linearly proportional to I_l in both regimes. The anti-Stokes to Stokes ratio, $\rho = S(\omega_{aS})/S(\omega_S)$, thus changes from a constant value proportional to n_b^{th} in the thermal regime, to being linearly dependent on I_l in the vibrational pumping regime. The characteristic Stokes and anti-Stokes emissions in the thermal and vibrational pumping regimes, as obtained within the QMO, are shown in Fig. 3(b) and (c) respectively (blue lines) for $I_l < 100$ μW μm^{-2}.

Furthermore, for the largest coherent pumping investigated in Fig. 3, we find that the phonon populations, as well as the Stokes and anti-Stokes intensities, deviate from the typical behaviour associated with the vibrational pumping regime given by the right-hand side of eqn (40), showing a clear nonlinear dependency. This is a result of the interplay of the two mechanisms pointed out in the beginning of this section: (i) phonon-stimulated emission, found when the phonon population $n_{\delta b}$ approaches unity, and (ii) parametric instability occurring when the optomechanical damping Γ_{opt} is negative and comparable to γ_m.

To isolate the effect of the first mechanism, we consider the case of the laser tuned to the cavity resonance, $\Delta = 0$, which ensures that the optomechanical damping Γ_{opt} vanishes. As we have shown in eqn (23), in this case we can still build up the phonon population through vibrational pumping ($n_{\delta b} \propto I_l$) until it becomes comparable to 1. Consequently, the Stokes emission $S(\omega_S) \propto |\alpha|^2(1+n_{\delta b})$

gains a contribution proportional to I_l^2. This can be considered as a new regime of phonon-stimulated Raman scattering, which, for $\Delta = 0$, is characterized by a quadratic dependence of the Stokes signal on the laser intensity.[10]

The behavior of the system induced by the second mechanism, namely parametric instability, is even more dramatic. For negative detuning of the incident laser $\Delta < 0$, when Γ_{opt} becomes comparable to the vibrational losses, γ_m, the denominator in eqn (21) tends to zero and the phonon population diverges. This regime of parametric instability has been studied and analyzed in other optomechanical systems, and may be more easily achievable in SERS configurations through pulsed illumination, to ensure that the strong laser does not damage the plasmonic substrate.[28]

2.4.2 Power dependence in CMO. As we have briefly mentioned earlier, the classical optomechanical model, unlike QMO, does not account for the fact that the vibrational ladder can be directly populated through Stokes transitions. Consequently, for typical SERS systems ($n_{\delta b} \ll 1$ and $|\Gamma_{opt}| \ll \gamma_m$) the phonon population $n_b^{(CMO)}$ (eqn (34)) does not exhibit an obvious dependence on the power of the incident laser, as in the case of the QMO (eqn (39)). Nevertheless, we can identify a more subtle dependence associated with the optomechanical damping Γ_{opt} by expanding the definition of $n_b^{(CMO)}$:

$$n_b^{(CMO)} = \frac{\gamma_m}{\gamma_m + \Gamma_{opt}} n_b^{th} \approx \left(1 - \frac{\Gamma_{opt}}{\gamma_m}\right) n_b^{th}. \tag{41}$$

We illustrate this behavior with orange solid and dashed lines in Fig. 3(a), which correspond to blue-detuned ($\Delta = -\omega_m$) and resonant ($\Delta = 0$) laser illumination. In the former case (solid orange line), we observe a considerable amplification only for very strong illumination, previously discussed in the context of parametric instability. Furthermore, for the laser tuned to the cavity resonance (dashed orange line), a constant phonon population given by the temperature of the system is obtained, $n_b^{(CMO)} = n_b^{th}$. One can thus conclude that this formulation of the CMO effectively does not include any mechanism equivalent to vibrational pumping.

The Stokes $S^{(CMO)}(\omega_S)$ and anti-Stokes $S^{(CMO)}(\omega_{aS})$ emission intensities in Fig. 3(b) and (c), respectively, show a behaviour similar to that found in the QMO (eqn (40):

$$\begin{aligned} S^{(CMO)}(\omega_S) &\propto |\alpha|^2 \left(1 + n_b^{(CMO)}\right), \\ S^{(CMO)}(\omega_{aS}) &\propto |\alpha|^2 n_b^{(CMO)}. \end{aligned} \tag{42}$$

However, as the phonon population does not significantly increase with I_l until it approaches the instability regime, the Stokes and anti-Stokes emissions are characterized for typical laser intensities by an almost constant, linear dependency on I_l which we previously identified as a thermal pumping regime. Consequently, their intensity ratio should not vary significantly from

$$\frac{S^{(CMO)}(\omega_{aS})}{S^{(CMO)}(\omega_S)} = \frac{\Gamma_-}{\Gamma_+} \left(\frac{\omega_{aS}}{\omega_S}\right)^4 \frac{n_b^{th}}{1 + n_b^{th}}. \tag{43}$$

This suggests that in typical SERS experiments, the estimation of the anti-Stokes signal within the CMO should remain very weak, thus preventing the observation of significant anti-Stokes emission at 10 K, contrary to the evidence recently reported.[13]

We have thus shown that the CMO does not describe the vibrational pumping of phonons. Therefore, reaching phonon populations nearing unity, required to observe phonon-stimulated emission, would only be possible within a CMO scheme through the mechanism of parametric instability.

2.5 Optomechanical models facing experimental results: vibrational pumping and local heating

2.5.1 QMO *vs.* CMO in plasmonic picocavities. We can further compare the predictions of the two optomechanical models with recent experimental results obtained in a well-defined SERS system.[13] In particular, the SERS signal from molecules placed in the gap between a gold nanoparticle and a gold substrate can be obtained in great detail, and Raman spectra of specific vibrational lines can be monitored as a function of the power of the incident illumination. Here we focus on a situation where atomic-scale hot spots – 'picocavities' – are produced by atomic protrusions at the nanoscale gap, and study the dependence of the anti-Stokes to Stokes ratio on the incident laser power. We use reasonable parameters to describe both the molecules as well as the plasmonic picocavity used in the experimental studies. It should be noted that the optical response of the system discussed in ref. 13 deviates somewhat from the single Lorentzian resonance picture discussed until now, and it includes contributions from additional, higher energy plasmon modes. While these modes could play a role in the modification of the phonon dynamics, through power-independent modifications of Stokes and anti-Stokes rates, we expect that the effect of these modes will not change the general trends and qualitative behavior presented here.

In Fig. 4 we present the experimental results for the ratio $\tilde{S}(\omega_{aS})/\tilde{S}(\omega_S)$ of a specific vibrational mode of a molecule in the proximity of a picocavity (blue dots) at cryogenic temperature ($T = 10$ K).[13] A calculation of this ratio within the QMO (eqn (28)) is shown with a blue solid line, yielding good agreement with the experimental observations when a coupling parameter $\hbar g_0 = 16$ meV is used. Both the experimental data and the results of the QMO model find the anti-Stokes/Stokes ratio to be proportional to the incident laser power I_l. This dependency is a characteristic of the vibrational pumping regime, as discussed in the previous subsections.

As shown earlier, within the CMO, the anti-Stokes emission is suppressed at a nominal temperature of $T = 10$ K, and thus this model would predict a much lower value of the $\tilde{S}(\omega_{aS})/\tilde{S}(\omega_S)$ ratio. For the sake of comparison, we also perform calculations within the CMO (eqn (37)) at temperatures of 250 K and 300 K (room temperature) with the same coupling parameter $\hbar g_0 = 16$ meV. The corresponding thermal populations are 0.01 (orange dashed line) and 0.02 (red dashed line), respectively. Increasing the thermal population does yield a larger anti-Stokes to Stokes ratio (from the orange to red dashed lines), but it still remains nearly constant for the considered pumping powers. We also consider an increased value of the coupling strength (32 meV, the green dashed line) which yields

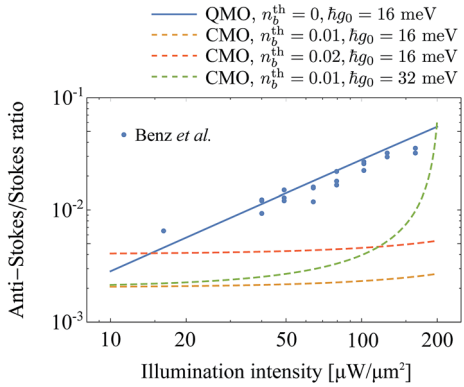

Fig. 4 Comparison of the anti-Stokes to Stokes ratios calculated by application of the QMO (eqn (28), blue solid line) and the CMO (eqn (37), dashed lines) models. We include recent experimental data from Benz *et al.*[13] obtained in a plasmonic gap under cryogenic conditions. For the QMO model, the coupling parameter was fitted to the experimental results. For the CMO model, we consider the emission ratios obtained by increasing the thermal population n_b^{th} (orange and red dashed lines) and coupling parameter (green dashed line). All the remaining parameters used were taken from ref. 13.

a much more dramatic increase of the anti-Stokes emission than in the experimental results, approaching the instability regime. The absence of a proper treatment of the pumping regime in the CMO thus seems to prevent recovering the linear dependence of the anti-Stokes/Stokes ratio observed in this experiment.

2.5.2 Role of local heating. It might be tempting to address experimental anti-Stokes to Stokes ratios by considering the mechanism of local heating of the molecule and its immediate environment by the incident laser. This effect was discussed at length in the literature on SERS,[29–32] and recognized as a relevant contribution to the power dependence of anti-Stokes emission. To estimate the local temperature changes required to considerably alter the phonon population, we plot the thermal population of phonons, n_b^{th}, in Fig. 5(a) for a range of typical vibrational frequencies and temperatures of interest. We can observe that while for very low temperatures the thermal population grows rapidly with T, the overall populations in these thermal regimes are very low, $n_b^{th} < 10^{-2}$. For a system at room temperature (green line in Fig. 5(a)), the increase of T required to double the phonon population varies from $\Delta T = 120$ K (solid vertical line in Fig. 5(a)) to $\Delta T = 50$ K (dashed vertical line in Fig. 5(a)) for vibrational energies of $\hbar\omega_m = 50$ meV and 150 meV, respectively. We note that in the latter case, the thermal population at 350 K would still be below 10^{-2}. This simple analysis indicates that any significant phonon population would require dramatic localized heating to occur.

An interesting approach for studying the local heating effect relies on the observation of the dependence of the Raman scattering on the incident laser power I_l. If the local heating were to form a reliable alternative mechanism of phonon population build-up, as compared to vibrational pumping, it should yield a clear, quadratic dependence of the anti-Stokes emission, and a linear dependence of the phonon population (and thus the anti-Stokes to Stokes ratio), on I_l.

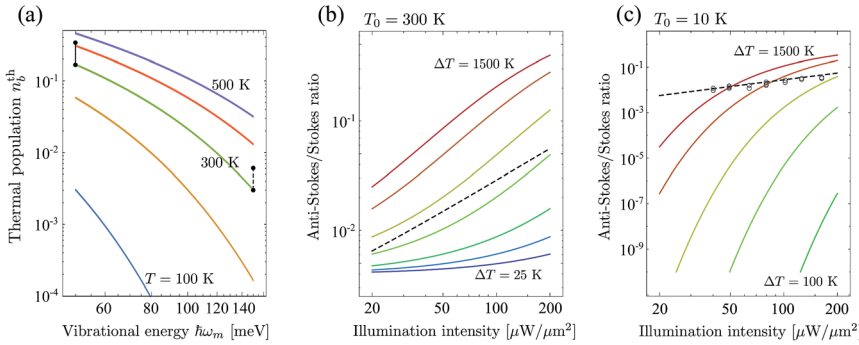

Fig. 5 (a) Thermal population n_b^{th} as a function of vibrational energy $\hbar\omega_m$ for different temperatures T, from 100 to 500 K. Vertical solid and dashed lines indicate the temperature increase required to double the thermal population of a mode with a vibrational energy of 50 or 150 meV, respectively. (b and c) Ratio of anti-Stokes to Stokes emission $\tilde{S}(\omega_{aS})/\tilde{S}(\omega_S)$ as the intensity of the incident laser is increased, assuming that the phonon population is dominated by the thermal contribution. We assume that the sample is heated by the incoming light, with the increase of temperature linear with the laser intensity (see eqn (44)). The initial temperature of the sample is $T_0 = 300$ K in (b) and $T_0 = 10$ K in (c). The different colors of the solid lines correspond to different values of absolute temperature increase, chosen so that ΔT at the maximum intensity shown for each line corresponds to $\Delta T = 25$ K, 50 K, 100 K, 250 K, 500 K, 1000 K and 1500 K (from the blue to the red line as ΔT increases). The black dashed line indicates the anti-Stokes to Stokes ratio obtained when the phonon population is dominated by vibrational pumping. The gray circles correspond to the experimental ratios $\tilde{S}(\omega_{aS})/\tilde{S}(\omega_S)$, measured for a molecule placed in a picocavity at cryogenic temperatures (10 K).[13] The vibrational energy in the calculations and experiments is $\hbar\omega_m = 144$ meV.

Such a possibility can be explored by explicitly including a linear dependence of the local temperature on I_l above a background T_0, as[33,34]

$$T = T_0 + \Delta T = T_0 + \xi I_l, \tag{44}$$

where ξ is a linear coefficient of temperature increase. Under this assumption, the phonon population, $n_b^{th}(T)$, depends on the temperature, and the anti-Stokes emission is proportional to $I_l n_b^{th}(T)$. In Fig. 5(b) and (c) we show the ratio of the anti-Stokes to Stokes emission, $\tilde{S}(\omega_{aS})/\tilde{S}(\omega_S)$ as a function of the intensity of the incident laser, assuming that the phonon population is dominated by the thermal contribution. In this case, the anti-Stokes to Stokes ratio $\tilde{S}(\omega_{aS})/\tilde{S}(\omega_S) \approx \Gamma_-/\Gamma_+ \cdot n_b^{th}(T)/(1 + n_b^{th}(T))$. For simplicity we neglect the $(\omega_{aS}/\omega_S)^4$ prefactor, and consider the vanishing detuning case ($\Delta = 0$), where $\Gamma_+ = \Gamma_-$. An initial temperature $T_0 = 300$ K (room temperature) is considered in Fig. 5(b), whereas a cryogenic temperature $T_0 = 10$ K is used in Fig. 5(c). Different increases of the molecule–cavity temperature can be accounted for (under the same laser intensity increase) by modifying the value of the linear dependence through the parameter ξ. From the blue to the red line we assume a maximum increase of the temperature $\Delta T = 25$ K, 50 K, 100 K, 250 K, 500 K, 1000 K and 1500 K, respectively. At room temperature (Fig. 5(b)), an increase in temperature below 100 K (blue lines) cannot reproduce the linear anti-Stokes to Stokes ratio, and only for temperature increases of the order of 500 K and larger (red lines) can a certain similarity with the

linear behavior be approached, with a tendency to saturate with increasing incident intensity. However, the experimental temperature increase associated with strong illumination has been reported to be relatively small for certain plasmonic systems.[30,35] These experimental results are consistent with recent theoretical work by Khorashad *et al.*[36] on localized heating in hot-spots of plasmonic dimers, which estimates a temperature increase of up to 5 K for large laser intensities of 10^4 W cm^{-2}, and of 40 K for optimized dimer structures with a nanorod in the gap. These systems might be taken as representative of typical SERS setups, however one cannot discard strongly inhomogenous situations that might thermally isolate the molecule–cavity system and thus produce extreme local heating conditions. Furthermore, a different model of local heating of the molecule has been proposed in the literature,[30] based on the mechanism of thermalization between different vibrationally pumped modes of the molecule. Under normal conditions though, temperature increases below 100 K seem reasonable, thus preventing the emergence of a linear anti-Stokes to Stokes ratio by pure thermal effects in such a case. Thus, for a reasonable increase of temperature ΔT of the order of a few tens of K, the thermal approach fails to reproduce the linear increase of the phonon population (quadratic anti-Stokes intensity) with I_l.

The situation becomes even more extreme in the case of a cryogenic initial temperature ($T_0 = 10$ K) of the molecule–cavity system. In Fig. 5(c) we show how a temperature increase of even up to 1500 K (red line) in such a cryogenic situation fails to reproduce the linear anti-Stokes to Stokes ratio (straight dashed line), as obtained within the description of the quantum molecular optomechanical (QMO) model (eqn (28)). For comparison, we also include here as gray open circles the experimental results shown earlier in Fig. 4, regarding the evolution of the anti-Stokes to Stokes ratio of a molecular fingerprint in a picocavity at cryogenic temperature.[13] We note that these experimental points match the theoretical prediction obtained from the QMO (dashed line). Within the alternative mechanism of phonon population due to local heating, as explored here (coloured lines in Fig. 5(c)), an increase of the maximum temperature of a few hundred degrees (green lines) would provide an even worse description of the aS/S ratio in this cryogenic situation than for room temperature. In particular, if one considered an increase of the maximum temperature smaller than 100 K (not shown in Fig. 5(c)), the values of the ratio would fall well below the detection limit. The cryogenic picocavity thus serves as a nice benchmark to test thermal *versus* vibrational pumping regimes in a well-controlled cavity.

3 Phenomenological semi-classical (PSC) model

In this section we briefly introduce the phenomenological semi-classical (PSC) model which has been developed over the last two decades, and successfully applied to interpret numerous SERS experiments. As a starting point we choose the definition of the linear optical polarizability α_L introduced earlier in eqn (4), explicitly dependent on the normal mode coordinate Q_k and the Raman tensor R_k. Classically, the electric dipole induced in the molecule with polarizability α_L by the incident electromagnetic field oscillating at frequency ω_l is given by

$$\begin{aligned} p(t) &= (L_m)^{1/4}\alpha_L(Q_k)\mathbf{E}(\mathbf{r}_m, t) \\ &= (L_m)^{1/4}\alpha_L(0)\mathbf{E}(\mathbf{r}_m, t) + (L_m)^{1/4}Q_k(t)R_k\mathbf{E}(\mathbf{r}_m, t). \end{aligned} \quad (45)$$

Thus, if Q_k oscillates at frequency ω_m, the second term in the above equation is the Raman dipole, which oscillates at frequencies $\omega_l \pm \omega_m$, resulting in the Stokes and anti-Stokes scattering. Eqn (45) is analogous to eqn (3) in the quantum treatment, with the same values for R_k in both approaches.

The Stokes σ_S^0 and anti-Stokes σ_{aS}^0 cross-sections for Raman processes in the absence of the enhancement, $K(\omega)$, are:[17]

$$\sigma_S^0 = \frac{8\pi}{3}\left(\frac{Q_k^0 R_k}{4\pi\varepsilon_0 c^2}\right)^2 {\omega_S}^4 L_m\left(1 + n_b^{(PSC)}\right), \tag{46}$$

$$\sigma_{aS}^0 = \frac{8\pi}{3}\left(\frac{Q_k^0 R_k}{4\pi\varepsilon_0 c^2}\right)^2 {\omega_{aS}}^4 L_m n_b^{(PSC)}. \tag{47}$$

where $\omega_S = \omega_l - \omega_m$ and $\omega_{aS} = \omega_l + \omega_m$ are the frequencies of Stokes and anti-Stokes emission, respectively, and c is the speed of light in vacuum. Here $n_b^{(PSC)}$ describes the population of phonons, irrespective of whether they originate from the thermal excitation by the environment, or from the Stokes transitions. In the weak pumping regime, the former contribution n_b^{th} dominates, and the ratio between anti-Stokes and Stokes emission can be used as a probe of temperature:

$$\frac{\sigma_{aS}^0}{\sigma_S^0} = \left(\frac{\omega_{aS}}{\omega_S}\right)^4 \frac{n_b^{th}}{1 + n_b^{th}}. \tag{48}$$

In the semi-classical picture, the enhancing effect of plasmons affects the signal through two different mechanisms:[2,3,37–39] a stronger excitation rate due to the plasmonic field enhancement $|K(\omega_l)|^2$ at the frequency of the incident laser ω_l on the one hand, and an accelerated emission of Stokes or anti-Stokes photons on the other hand. In typical cases where reciprocity applies,[40] the latter effect equals the square of the plasmonic field enhancement $|K(\omega_l \pm \omega_m)|^2$ at the emission frequency. Both enhancement factors are related to the field projection on the Raman dipole induced in the molecule. We therefore arrive at

$$\sigma_S^{(PSC)} = \frac{8\pi}{3}\left(\frac{Q_k^0 R_k}{4\pi\varepsilon_0 c^2}\right)^2 {\omega_S}^4 L_m\left(1 + n_b^{(PSC)}\right)|K(\omega_l)|^2|K(\omega_S)|^2, \tag{49}$$

$$\sigma_{aS}^{(PSC)} = \frac{8\pi}{3}\left(\frac{Q_k^0 R_k}{4\pi\varepsilon_0 c^2}\right)^2 {\omega_{aS}}^4 L_m n_b^{(PSC)}|K(\omega_l)|^2|K(\omega_{aS})|^2. \tag{50}$$

Note that here again the phonon population $n_b^{(PSC)}$ will be modified due to the different rates of Stokes and anti-Stokes processes occurring in the molecule. We can divide the population into a part due to the thermal contribution n_b^{th}, and a part originating from Stokes transitions. The latter can be obtained by noting than every Stokes transition will create a phonon – the rate of this process can be calculated as the Stokes emission power $P_S = \sigma_S^{(PSC)} I_l$ divided by Stokes photon energy $\hbar\omega_S$, yielding

$$n_b^{(PSC)} = n_b^{th} + \frac{1}{\gamma_m \eta(\omega_S)} \frac{\sigma_S^{(PSC)} I_l}{\hbar\omega_S}. \tag{51}$$

We have introduced the radiative yield $\eta(\omega_S)$ of the Stokes emission to account for non-radiative processes which accelerate the rate of phonon creation, but do not lead to the emission of Stokes photons into the far-field, and thus are not included in $\sigma^{(PSC)}$. These effects were discussed in the literature, and experimentally proven to be significant.[41,42] For a single Lorentzian plasmonic mode the radiative yield should be constant, and thus we will drop the explicit dependence on frequency from the subsequent equations.

Furthermore, we can describe this phonon pumping mechanism by introducing the flux of the incoming photons n_l, defined by the incident illumination power density I_l as $n_l = I_l/(\hbar\omega_l)$:

$$n_b^{(PSC)} = n_b^{th} + \frac{\sigma_S^{(PSC)}}{\gamma_m \eta}\frac{\omega_l}{\omega_S} n_l. \tag{52}$$

This expression differs slightly from the one used in the literature (see ref. 31), as it explicitly accounts for the non-unitary radiative yield η and the lower energy of photons making up the scattered light ($\hbar\omega_S$) compared to the incident illumination ($\hbar\omega_l$).

The dependence of $\sigma_S^{(PSC)}$ on $n_b^{(PSC)}$, which itself depends on the cross section (eqn (52)) suggests that a feedback mechanism, reminiscent of that discussed in the context of the QMO and CMO, can be also identified in this classical treatment. In fact, as indicated by the early work of Kneipp *et al.*,[43] eqn (52) is equivalent to the steady state solution of the following rate equation for the total phonon population:

$$\frac{dn_b^{(PSC)}}{dt} = -n_b^{(PSC)}\gamma_m + \frac{\sigma_S^{(PSC)}}{\eta}\frac{\omega_l}{\omega_S} n_l + \gamma_m n_b^{th}. \tag{53}$$

Furthermore, we note that the phonons are not only created through Stokes transitions, but also removed from the molecule with each anti-Stokes transition. However, this latter effect is not taken into account in eqn (53). We discuss in Section 3.1.2 an appropriate extension of the PSC model that can indeed lead to a direct mapping between the PSC and the QMO approaches.

3.1 Comparison between PSC and QMO

In this section we show how the description of vibrational pumping, clearly described within the PSC model, can be expressed in terms of the parameters used in the molecular optomechanics and *vice versa*. Afterwards, we discuss an extension of the PSC which includes the effect of depletion of the phonon population by the anti-Stokes processes, and show that this approach leads to rate equations equivalent to those derived earlier within the QMO, and consequently, to a consistent threshold for instability.

3.1.1 Phonon populations for zero detuning. We begin by showing the identity between the expressions for the vibrationally-pumped phonon population, $n_b^{(vp)}$, derived in the PSC and those in the QMO, in the limit of weak optomechanical coupling $|\Gamma_{opt}| \ll \gamma_m$ and sufficiently low phonon populations. Within the PSC, this population is given by the second term in eqn (52):

$$n_{\mathrm{b}}^{(\mathrm{vp})} = \frac{\sigma_{\mathrm{S}}^{(\mathrm{PSC})}\omega_{\mathrm{l}} n_{\mathrm{l}}}{\eta\gamma_{\mathrm{m}}\omega_{\mathrm{S}}}. \tag{54}$$

Plugging in the definition of the Stokes cross-section $\sigma_{\mathrm{S}}^{(\mathrm{PSC})}$ from eqn (49), we get

$$n_{\mathrm{b}}^{(\mathrm{vp})}\Big|_{\mathrm{low\ I}} = \frac{n_{\mathrm{l}}}{\gamma_{\mathrm{m}}\eta}\frac{8\pi}{3}\left(\frac{R_{\mathrm{k}}Q_{\mathrm{k}}^{0}}{4\pi\varepsilon_{0}c^{2}}\right)^{2}\omega_{\mathrm{l}}{\omega_{\mathrm{S}}}^{3}L_{\mathrm{m}}|K(\omega_{\mathrm{l}})|^{2}|K(\omega_{\mathrm{S}})|^{2}, \tag{55}$$

where we include the subscript $|_{\mathrm{low\ I}}$ to stress that the phonon population is much smaller than unity ($n_{\mathrm{b}}^{(\mathrm{PSC})} \ll 1$). For a direct correspondence with the optomechanical model, we consider a single plasmon mode characterized by a frequency-dependent field enhancement, K, with a Lorentzian profile of resonant frequency ω_{c} and width κ:

$$|K(\omega)|^{2} = |K(\omega_{\mathrm{c}})|^{2}\frac{(\kappa/2)^{2}}{(\omega-\omega_{\mathrm{c}})^{2}+(\kappa/2)^{2}}. \tag{56}$$

Next, for simplicity we neglect the effects of relative permittivity, assuming $\varepsilon = L_{\mathrm{m}} = 1$. The vibrationally-pumped phonon population is then determined from eqn (52) as

$$n_{\mathrm{b}}^{(\mathrm{vp})}\Big|_{\mathrm{low\ I}} = \frac{8\pi{\omega_{\mathrm{S}}}^{3}\omega_{\mathrm{l}}}{3\gamma_{\mathrm{m}}\eta}\left(\frac{R_{\mathrm{k}}Q_{\mathrm{k}}^{0}}{4\pi\varepsilon_{0}c^{2}}\right)^{2}|K(\omega_{\mathrm{c}})|^{4}n_{\mathrm{l}}\frac{\kappa^{2}}{4\Delta^{2}+\kappa^{2}}\frac{\kappa^{2}}{4(\Delta+\omega_{\mathrm{m}})^{2}+\kappa^{2}}. \tag{57}$$

The first parenthesis on the right-hand side can be expressed in terms of the square of the optomechanical single-photon coupling g_0 and the effective volume V (eqn (10)). We assume, as in Section 2.1, that the molecule is optimally positioned and oriented so that the spatial parameters $|u(\mathbf{r}_{\mathrm{m}})|^{2}(\mathbf{u}_{\mathrm{E}}\cdot\mathbf{u}_{\mathrm{k}})^{2} = 1$. The expression for the field enhancement $K(\omega_{\mathrm{c}})$ can be related with the Purcell factor, P_{F}, following $|K(\omega_{\mathrm{c}})|^{4} = {P_{\mathrm{F}}}^{2}\eta^{2}$, which can in turn be expressed[10] through the effective mode volume V as

$$P_{\mathrm{F}} = \frac{6\pi c^{3}}{V\kappa{\omega_{\mathrm{c}}}^{2}}. \tag{58}$$

Furthermore, as we show in Appendix B, the flux n_{l} of incident photons populates the molecule with the coherent amplitude $\alpha \approx 2\Omega/(\kappa + 2\mathrm{i}\Delta)$, given in eqn (78). After some simple algebra, we arrive at the phonon population

$$\begin{aligned} n_{\mathrm{b}}^{(\mathrm{vp})}\Big|_{\mathrm{low\ I}} &= 4{g_{0}}^{2}\frac{\kappa}{\gamma_{\mathrm{m}}}\left(\frac{\omega_{\mathrm{S}}}{\omega_{\mathrm{c}}}\right)^{3}\frac{|\alpha|^{2}}{4(\Delta+\omega_{\mathrm{m}})^{2}+\kappa^{2}} \\ &= \left(\frac{\omega_{\mathrm{S}}}{\omega_{\mathrm{c}}}\right)^{3} n_{\delta\mathrm{b}}^{(\mathrm{vp})}\Big|_{\mathrm{low\ I}}. \end{aligned} \tag{59}$$

We thus obtain a similar expression for the population induced by vibrational pumping within the PSC model to the one derived using the QMO formalism in the limit of $n_{\delta\mathrm{b}} \ll 1$ and $|\Gamma_{\mathrm{opt}}| \ll \gamma_{\mathrm{m}}$ (the second term in eqn (39), denoted here as

$n_{\mathrm{sb}}^{(\mathrm{vp})}$). The differences in the expression relating both populations are given by the ratio of the frequencies $(\omega_{\mathrm{S}}/\omega_{\mathrm{c}})$,[3] which is close to unity in a typical system.

The direct connection between the expressions in the QMO and PSE models suggests that one should be able to obtain the optomechanical coupling constant g_0 from the classical Raman cross-section. Indeed, equating the vibrationally-pumped phonon population in PSC, $n_{\mathrm{b}}^{(\mathrm{vp})}$ (eqn (54)), with the same magnitude in QMO (second term in eqn (39)), and using again the relationship between n_{l} and α (eqn (78)), we obtain the following expression for the optomechanical coupling parameter:

$$g_0{}^2 = \sigma_{\mathrm{S}}^{(\mathrm{PSC})}\Big|_{\text{low I}} \frac{\omega_{\mathrm{c}}{}^3}{24\pi c^2\eta^2\kappa^2\omega_{\mathrm{S}}}\left(\kappa^2+4\Delta^2\right)\left[\kappa^2+4(\Delta+\omega_{\mathrm{m}})^2\right], \tag{60}$$

expressed in terms of the classical parameters defining the molecule and the plasmonic cavity. We note that the factors dependent on detuning cancel out with the respective enhancement factors included in the definition of cross section $\sigma_{\mathrm{S}}^{(\mathrm{PSC})}$, yielding a frequency-independent g_0.

3.1.2 Extension of the PSC model: approaching classical instability. Both optomechanical formalisms predict the onset on instability when the negative optomechanical damping Γ_{opt} becomes comparable to $-\gamma_{\mathrm{m}}$. As we have shown in Subsection 2.2.1, this result can be derived from a simple rate equation (eqn (20)) for the phonon populations in the framework of QMO.

Using the correspondence between the optomechanical and classical parameters used in QMO and PSC, we can now attempt to rewrite the rate equation derived in the QMO framework in terms of the cross-sections. To this end, we introduce classical analogues of the optomechanical transition rates, $\Gamma_{\pm}^{(\mathrm{PSC})}$, defined as

$$\Gamma_{+}^{(\mathrm{PSC})} = \frac{\sigma_{\mathrm{S}}^{(\mathrm{PSC})}}{1+n_{\mathrm{b}}^{(\mathrm{PSC})}}\frac{n_{\mathrm{l}}}{\eta}\frac{\omega_{\mathrm{l}}}{\omega_{\mathrm{S}}}, \quad \Gamma_{-}^{(\mathrm{PSC})} = \frac{\sigma_{\mathrm{aS}}^{(\mathrm{PSC})}}{n_{\mathrm{b}}^{(\mathrm{PSC})}}\frac{n_{\mathrm{l}}}{\eta}\frac{\omega_{\mathrm{l}}}{\omega_{\mathrm{aS}}}. \tag{61}$$

With these definitions, assuming $\Delta = \Delta'$ and using the value of $\sigma_{\mathrm{S}}^{(\mathrm{PSC})}$ in eqn (49), we can proceed similarly as in the previous subsection and obtain an expression of $\Gamma_{+}^{(\mathrm{PSC})}$ that relates with the QMO Γ_{+} in eqn (18) as

$$\Gamma_{+}^{\mathrm{PSC}} = \left(\frac{\omega_{\mathrm{S}}}{\omega_{\mathrm{c}}}\right)^3\Gamma_{+}. \tag{62}$$

Similarly, we can find from the definitions of $\sigma_{\mathrm{aS}}^{(\mathrm{PSC})}$ (eqn (50)) and Γ_{-} (eqn (19)) the analogous relationship

$$\Gamma_{-}^{(\mathrm{PSC})} = \left(\frac{\omega_{\mathrm{aS}}}{\omega_{\mathrm{c}}}\right)^3\Gamma_{-}. \tag{63}$$

With these definitions, the rate equation derived originally in the QMO framework (eqn (20)) translates into:

$$\frac{\mathrm{d}n_{\mathrm{b}}^{(\mathrm{PSC})}}{\mathrm{d}t} = -n_{\mathrm{b}}^{(\mathrm{PSC})}\left(\gamma_{\mathrm{m}}+\Gamma_{-}^{(\mathrm{PSC})}\right)+\left(n_{\mathrm{b}}^{(\mathrm{PSC})}+1\right)\Gamma_{+}^{(\mathrm{PSC})}+\gamma_{\mathrm{m}}n_{\mathrm{b}}^{\mathrm{th}}, \tag{64}$$

where for simplicity we have considered $\omega_S \approx \omega_c \approx \omega_{aS}$. Equivalently, expressing the rate equations through the cross sections (see eqn (62) and (63)), we can write:

$$\frac{dn_b^{(PSC)}}{dt} = -n_b^{(PSC)}\gamma_m - \frac{\sigma_{aS}^{(PSC)}}{\eta}\frac{\omega_l}{\omega_{aS}}n_l + \frac{\sigma_S^{(PSC)}}{\eta}\frac{\omega_l}{\omega_S}n_l + \gamma_m n_b^{th}. \quad (65)$$

We stress that the Raman cross-sections in this rate equation are dependent on the phonon population, as indicated in eqn (49) and (50). This equation can be considered as an extension of the phenomenological rate equation introduced in the beginning of the section (eqn (53)), as it accounts for the depletion of the phonon population due to the anti-Stokes processes, consistently with the previous work by Le Ru and Etchegoin.[30] Therefore, we find that the predictions of the QMO can again be interpreted in terms of classical Raman cross-sections and semi-classical descriptions, valid even near the instability regime for the case of an arbitrary plasmonic response (see Appendix C for a further discussion).

4 Outlook beyond the classical rate equations

As we have shown in the previous section, far from the instability ($|\Gamma_{opt}| \ll \gamma_m$) and phonon-stimulated ($n_b \ll 1$) regimes, the fundamental characteristics of SERS can be addressed rather well with a standard PSC formalism in terms of classical rate equations which provide a direct and intuitive picture of the phenomena contributing to the phonon population. In Section 3.1.2 we have shown that the extension of this framework to situations of strong vibrational pumping is also possible and can be used to introduce a semi-classical interpretation of the optomechanical damping. Indeed, the situations of strong pumping are very appealing to study in the context of SERS, since they yield large phonon populations and, consequently, give rise to significant anti-Stokes processes.

Nevertheless, the quantum-mechanical picture of Raman scattering in cavities allows us to discuss many other properties, such as the statistics of light emitted by the SERS systems, or the build-up of dissipation-mediated coherence between molecules positioned inside the cavities. The optomechanical framework also opens pathways to studying Raman scattering in systems where molecular vibrations are strongly coupled to plasmons. Below, we briefly review some of the most appealing perspectives, in our view, in the development of molecular optomechanics.

4.1 Optomechanical single-photon strong coupling regime

The large reported values of the single-photon coupling strength, g_0, in molecular optomechanics suggest that SERS can in fact be a valid optomechanical platform which might allow us to approach the optomechanical single-photon strong-coupling regime,[44,45] where $g_0 \geq \kappa$.

In Fig. 6(a) we present a graphical comparison of various optomechanical systems including SERS as a function of the two key optomechanical parameters: the single-photon coupling and decay rate of the cavity. While the criterion for single-photon strong coupling, $g_0 \approx \kappa$, appears to be very challenging for single-molecule SERS, where the largest reported coupling strength has been $g_0 \approx \kappa/10$,[13]

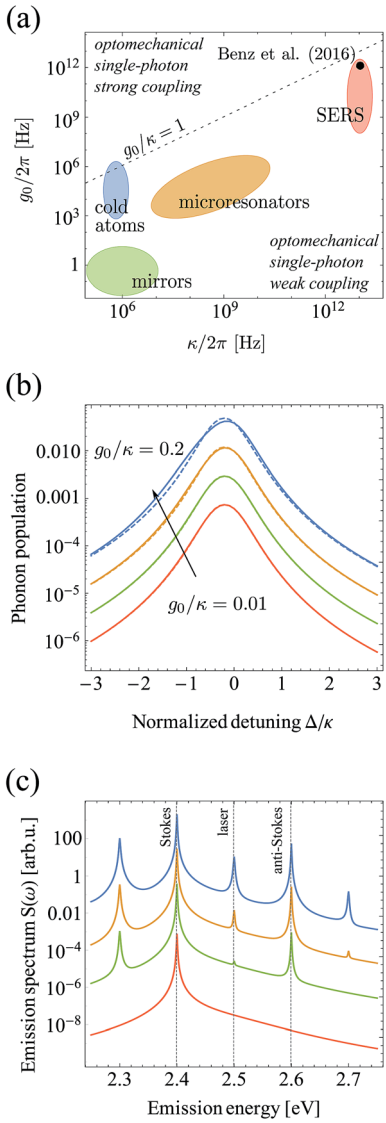

Fig. 6 Molecular optomechanics near the optomechanical single-photon strong coupling regime. (a) Schematic representation of the key parameters, g_0 and κ, in typical realizations of optomechanical systems, based on the original figure in ref. 11. (b) Phonon populations as a function of laser detuning, Δ, for normalized g_0/κ from 0.01 to 0.2. Solid and dashed lines denote the numerical solutions of the full (eqn (14)) and linearized (eqn (15)) optomechanical Hamiltonians. We have verified that the QMO model yields populations (eqn (21)) identical to those obtained by numerically solving the linearized Hamiltonian, hinting at the hierarchy of approximation leading to the QMO model. (c) Emission spectra from the optomechanical system driven on resonance, $\Delta = 0$. Coupling parameters are considered as in (b). All the calculations in (b) and (c) are carried out for weak pumping, $\Omega/\kappa = 0.02$.

this regime might be at hand by coupling to coherently coupled layers of molecules or to extended 2D systems.

We consider situations of SERS approaching single-photon coupling in Fig. 6(b) and (c). As observed for ratios of the coupling strength to cavity decay rate, g_0/κ, approaching a value of 0.2, neither the phonon populations (Fig. 6(b)), nor the emission spectra (Fig. 6(c)) exhibit any clear characteristics similar to those observed in resonantly coupled systems, such as mode splitting characteristic of a Jaynes–Cummings Hamiltonian, for instance. The most striking feature of the emission spectra in this regime might be the emergence of additional emission lines at $\omega_l \pm 2\omega_m$ and at ω_l, originating from two-phonon scattering events.

Dramatic changes can be observed when considering the two-photon correlations of the emitted light, which in the single-photon strong coupling regime can exhibit strong anti-bunching due to the photon blockade effect.[44,45] A systematic extension of the study of two-photon correlations towards the frequency-resolved correlation measurements will be presented elsewhere.[46]

4.2 Coupling between multiple molecules in the cavity

In the initial work on molecular optomechanics, Roelli *et al.*[9] suggested that a system comprising a collection of N identical molecules coupled optomechanically to one plasmonic cavity mode can be described by introducing a collective vibrational mode, with the coupling parameter scaling with $\sqrt{N}$. This approach can be generalized by considering the master equation for a collection of molecules coupled to a single cavity mode. In such a formulation, slightly modified Lindblad–Kossakowski terms, usually identified with dissipation, mediate the interactions between molecules, and provide a pathway to build up coherence between them. Similar systems, in which plasmon-mediated dissipative interactions would enable the build-up of entanglement between distant two-level emitters, have been discussed recently.[47] We can therefore consider that a similar phenomenon might be worthwhile to study in the context of optomechanical coupling, particularly in light of recent research devoted to the role of spatial coherence in extended, two-dimensional systems in TERS configurations.[48,49] This leads us to an interesting, and yet unanswered question of whether this effect can be found in realistic systems or whether it would be hidden when one considers that the molecules in a typical SERS system are not identical and that losses can hinder the coherence build-up.

4.3 Statistics of emission: SaS bunching and anti-bunching

The description of SERS in the fully quantum-mechanical framework opens a pathway to studying indicators of the non-classical characteristics of the system. The correlation of the emission of Stokes and anti-Stokes photons (SaS correlations[5,6]) can be traced by accessing the frequency-resolved second-order correlation function, $g^{(2)}_{\Gamma,\Gamma}(\omega_S,\omega_{aS})$, of the two-color emission, and the quantum nature of these correlations can be checked by means of the Cauchy–Schwarz inequalities. We previously found large two-photon correlations between the Stokes and anti-Stokes photons emitted from optical cavities weakly coupled to molecules.[10] It appears promising to study the non-classical anti-bunching observed between

emission features in systems approaching the single-photon strong coupling regime.[46]

4.4 Effect of anharmonicity on the instability

In the QMO formalism, the rate equations for the phonon population, eqn (20), resemble those describing the population inversion in lasing. Following this resemblance, we can directly formulate the phonon lasing threshold (parametric instability) as that determined by the vanishing of the effective phonon decay rate in eqn (21): $\gamma_m + \Gamma_{opt} \rightarrow 0$. This effect occurs thanks to the stimulated emission of phonons, described in the right-hand side of the rate equation in eqn (20) by the term $n_{\delta b}\Gamma_+$. Note that if we were to suppress it by taking $n_{\delta b} \ll 1$, the effective phonon population $n_{\delta b}$ would be given by $\Gamma_+/(\Gamma_- + \gamma_m)$ and could never reach lasing, as $\Gamma_- > 0$.

As we approach the instability regime, we invariably build up the phonon population and populate higher rungs of the vibrational ladder. The energies of these states increasingly diverge from those derived within the bosonic quantization of vibrations due to the anharmonicity of the energy potential (see Fig. 1(b)). This balance between the nonlinear build-up of phonon populations and the breakdown of the harmonic potential approximation should be expressed in the superlinear dependence of Stokes emission on the power of the incident laser.[30]

4.5 SERS as a platform for quantum cavity optomechanics

Finally, we note that from the perspective of researchers working in the field of optomechanics, SERS can be considered as a unique platform which provides unusual characteristics in this field:

- The possibility to approach single-photon strong coupling (see the discussion in Section 4.1).
- THz mechanical frequencies are unmatched by any other optomechanical system. Consequently, the vibrations are very weakly thermally populated (see Fig. 4(b)).
- Plasmonic cavities are notoriously difficult to populate, but they can provide very small effective mode volumes. Furthermore, these special cavities do not act as narrow filters for the cavity field and can therefore support sideband oscillations. Consequently, the vibrational state of the molecule can be measured directly through the observations of Stokes and anti-Stokes peaks, without the need to employ additional probe beams.

5 Concluding remarks

The process of Raman scattering is intrinsically quantum-mechanical, as it describes transitions between discrete vibrational levels of a molecule. On the other hand, quantization of the electromagnetic field of a nanocavity, which offers enhancement of Raman scattering, might seem unnecessary, as long as the considered cavity is pumped by coherent illumination and does not dissipate its excitations in a non-linear fashion. Indeed, the framework in which the classical description of the plasmonic resonance is utilized has been successfully applied to describe SERS for over two decades. It is only when the sophistication of

synthetic and fabrication techniques have made it possible to carefully engineer both molecular morphologies and locations in exquisite plasmonic cavities, that the intrinsic quantum-mechanical nature of a surface-enhanced Raman process may be revealed.

In this work we attempted to explore some limitations of the classical treatment of SERS, and confront them with the predictions of the recently proposed formalism of molecular optomechanics. In the regime of parameters which correspond to the majority of experimental SERS setups, we find that the solutions offered by the quantum molecular optomechanics are indeed consistent with those given by the well-established PSC model. In particular, within the quantum molecular (QMO) model we correctly reproduce the elementary characteristics of Raman scattering, namely the dependence of the Raman signal on the power and frequency of the incident laser, and on the temperature.

Additionally, molecular optomechanics offers us insights into the characteristics of Raman scattering which are not readily addressed with the PSC model. These include the onset of phonon-stimulated processes, the amplification and cooling of phonon populations, and finally the parametric instability. Interestingly, as we show above, all of these processes can be included in a classical framework in an *ad hoc* manner, complementing the previous analysis of the population of the vibrational ladder.[30] In particular, the rate equations for the phonon population derived within the PSC formalism can be extended to reflect the exact form of the corresponding equations in the quantum optomechanical framework.

The regime of parameters where these effects could become directly accessible has seemingly only recently been reached through the careful engineering of plasmonic cavities,[13,50] alignment of the molecules, or the use of pulsed, high-power lasers which avoid melting the plasmonic particles.[28,32] This progress has been further stimulated by the discovery of new effects, such as the formation of atomic-sized protrusions inside the plasmonic cavities.[13,51,52]

Additional experimental efforts should help us to study the fundamental properties of the Raman processes, which are directly and naturally addressed by quantum molecular optomechanics. Potential experiments might include the investigation of non-classical correlations of the scattered light, or studies of the intermolecular coherence build-up in plasmonic cavities. SERS systems can also be an attractive platform for the optomechanical community, as they might access the regime of optomechanical single-photon strong coupling.

A Linearization of the optomechanical Hamiltonian

Consider the Hamiltonian given by eqn (8) in the main text in the frame rotating with the frequency of the laser ω_l ($\Delta = \omega_c - \omega_l$):

$$\hat{H} = \hbar\Delta\hat{a}^\dagger\hat{a} + \hbar\omega_m\hat{b}^\dagger\hat{b} + i\hbar\Omega(\hat{a}^\dagger - \hat{a}) - \hbar g_0\hat{a}^\dagger\hat{a}(\hat{b} + \hat{b}^\dagger). \quad (66)$$

The Heisenberg–Langevin equations for the dynamics of the cavity $\hat{a}$ and vibrations $\hat{b}$ operators, derived from this Hamiltonian, are

$$\dot{\hat{a}} = -(\kappa/2 + \mathrm{i}\Delta)\hat{a} + \mathrm{i}g_0\hat{a}\left(\hat{b} + \hat{b}^\dagger\right) + \Omega + \sqrt{\kappa}a_{\mathrm{in}}(t), \tag{67}$$

and

$$\dot{\hat{b}} = -(\gamma_{\mathrm{m}}/2 + \mathrm{i}\omega_{\mathrm{m}})\hat{b} + \mathrm{i}g_0\hat{a}^\dagger\hat{a} + \sqrt{\gamma_{\mathrm{m}}}b_{\mathrm{in}}(t), \tag{68}$$

with noise terms

$$\langle\hat{a}_{\mathrm{in}}(t)\rangle = 0,\ \langle\hat{a}_{\mathrm{in}}(t)\hat{a}^\dagger_{\mathrm{in}}(t')\rangle = \delta(t - t'), \tag{69}$$

and

$$\langle\hat{b}_{\mathrm{in}}(t)\rangle = 0,\ \langle\hat{b}^\dagger_{\mathrm{in}}(t)\hat{b}_{\mathrm{in}}(t')\rangle = n_{\mathrm{b}}^{\mathrm{th}}\delta(t - t'). \tag{70}$$

We can displace the operators $\hat{a}$ and $\hat{b}$ by arbitrary coherent amplitudes α and β, respectively, and rewrite the above equations putting $\hat{a} = \alpha + \delta\hat{a}$ and $\hat{b} = \beta + \delta\hat{b}$. If we choose the coherent amplitudes as

$$\alpha = \frac{\Omega}{\kappa/2 + \mathrm{i}[\Delta - 2g_0\mathrm{Re}(\beta)]} = \frac{\Omega}{\kappa/2 + \mathrm{i}\Delta'}, \quad \beta = \frac{g_0|\alpha|^2}{\omega_{\mathrm{m}} - \mathrm{i}\gamma_{\mathrm{m}}/2}, \tag{71}$$

drop the small terms with quadratic dependence on fluctuations $\delta\hat{a}^\dagger\delta\hat{b}$, $\delta\hat{a}^\dagger\delta\hat{b}^\dagger$ and $\delta\hat{a}^\dagger\delta\hat{a}$, from these equations, and rotate the cavity operators by $\arg(\alpha)$ (see discussion following eqn (13)), the dynamics of fluctuations will be simplified to

$$\dot{\delta\hat{a}} = -\left(\kappa/2 + \mathrm{i}\Delta'\right)\delta\hat{a} + \mathrm{i}g\left(\delta\hat{b} + \delta\hat{b}^\dagger\right) + \sqrt{\kappa}a_{\mathrm{in}}(t), \tag{72}$$

$$\dot{\delta\hat{b}} = -(\gamma_{\mathrm{m}}/2 + \mathrm{i}\omega_{\mathrm{m}})\delta\hat{b} + \mathrm{i}g\left(\delta\hat{a} + \delta\hat{a}^\dagger\right) + \sqrt{\gamma_{\mathrm{m}}}b_{\mathrm{in}}(t). \tag{73}$$

These equations correspond to the dynamics given by the linearized Hamiltonian in eqn (15). Since there are no coherent driving terms in these equations, the expectation values of the fluctuations in the steady state will vanish $\langle\delta a\rangle_{\mathrm{ss}} = \langle\delta b\rangle_{\mathrm{ss}} = 0$. The above Heisenberg–Langevin equations can be solved exactly for only a few cases ($\Delta' = 0$ or $\pm\omega_{\mathrm{m}}$) (see the SI in ref. 10).

An approximated solution to eqn (72) and (73) for arbitrary detuning Δ was found by Wilson-Rae *et al.*,[22] and Marquardt *et al.*[23] when searching for the lower limits of the sideband cooling technique. Both these contributions are based on the adiabatic elimination of the optical degree of freedom and solving the resulting master equation for the dynamics of vibrations in presence of the cavity, whose sole role is the modification of the transition rates between vibrational levels. This solution is then inserted into the expression for the emission spectrum (eqn (25)). For a detailed derivation, we direct the reader to an excellent discussion presented in ref. 24 and the equivalent approach, albeit limited to the resolved-sideband approximation $\omega_{\mathrm{m}} \gg \kappa$, presented by Wilson-Rae *et al.*[25]

Finally, for the sake of completeness, the expression for the change in vibrational frequency Δ_{m} (spring effect) discussed earlier, occurring due to the coupling of vibrations to the non-zero coherent amplitude of the plasmon is[11]

$$\Delta_{\mathrm{m}} = -\left(\Gamma_-\frac{\Delta' - \omega_{\mathrm{m}}}{\kappa} + \Gamma_+\frac{\Delta' + \omega_{\mathrm{m}}}{\kappa}\right). \tag{74}$$

Similarly as in the case of the optomechanical damping Γ_{opt}, the differences between this energy modification in QMO (where the coherent amplitude of the plasmon is α) and CMO (with amplitude $\alpha^{(\mathrm{CMO})}$) are negligible.

B Connection between the illumination parameters Ω and α

For the case of arbitrary detuning, the parameter Ω can be written as a function of the effective volume V, the incoming electric field E_0 and the plasmonic enhancement K evaluated at the plasmonic frequency and at the point outside the structure where the field is the strongest:[15]

$$\Omega = \frac{\kappa}{2}\sqrt{\frac{\varepsilon_0 V}{2\hbar\omega_{\mathrm{c}}}}|KE_0|. \tag{75}$$

We note that this definition was derived assuming a homogeneous incident field, a Lorentzian optical response and a dipolar emission pattern for the cavity. We assume as before that the dielectric function ε of the surrounding medium is equal to 1. To explicitly relate the effective mode volume V and the maximum field enhancement, we recall the relationship $P_{\mathrm{F}} = K^2/\eta$, and the expression for the Purcell factor offered by a single plasmonic mode, $P_{\mathrm{F}} = 6\pi c^3/(V\kappa{\omega_{\mathrm{c}}}^2)$. Furthermore, expressing the amplitude of the incident electric field E_0 through the power density $I_{\mathrm{l}} = c\varepsilon_0|E_0|^2/2$, we arrive at[10]

$$\Omega^2 = \frac{3\pi c^2\kappa\eta}{2\hbar{\omega_{\mathrm{c}}}^3} I_{\mathrm{l}}. \tag{76}$$

The power density is expressed by the incident photon flux as $I_{\mathrm{l}} = \hbar\omega_{\mathrm{l}} n_{\mathrm{l}}$, and thus

$$\Omega^2 = \frac{3\pi c^2\kappa\eta}{2}\frac{\omega_{\mathrm{l}}}{{\omega_{\mathrm{c}}}^3} n_{\mathrm{l}}. \tag{77}$$

The coherent amplitude α can be immediately obtained *via* the definition in eqn (13):

$$|\alpha|^2 = \frac{6\pi c^2\kappa\eta}{\kappa^2 + 4\Delta'^2}\frac{I_{\mathrm{l}}}{\hbar{\omega_{\mathrm{c}}}^3}, \quad \text{or} \quad |\alpha|^2 = \frac{6\pi c^2\kappa\eta}{\kappa^2 + 4\Delta'^2}\frac{\omega_{\mathrm{l}}}{{\omega_{\mathrm{c}}}^3} n_{\mathrm{l}}. \tag{78}$$

For a typical SERS setup, we can replace the effective Δ' with $\Delta = \omega_{\mathrm{c}} - \omega_{\mathrm{l}}$.

C Comparison with the generalized optomechanical model

Throughout this paper we have focused on the case where the response of the plasmonic cavity is completely characterized by a single quasi-Lorentzian resonance. We discuss now how our results compare with the expression derived recently by Dezfouli and Hughes[12] for an arbitrary plasmonic nanosystem. To do

so, we extend the rate equation for the phonon population introduced in the main text, so that it addresses the more general plasmonic situation. For simplicity, throughout this derivation we put $\varepsilon = L_m = 1$.

We first express the Raman cross-sections without considering reciprocity to address the effect of local field enhancement in the outgoing Raman photon. In such a case, eqn (49) and (50) need to be modified into

$$\sigma_S^{(PSC)} = \frac{8\pi}{3}\left(\frac{Q_k^0 R_k}{4\pi\varepsilon_0 c^2}\right)^2 {\omega_S}^4 |K(\omega_l)|^2 \frac{\Gamma^R(\omega_S)}{\Gamma_0(\omega_S)}\left(1 + n_b^{(PSC)}\right), \tag{79}$$

and

$$\sigma_{aS}^{(PSC)} = \frac{8\pi}{3}\left(\frac{Q_k^0 R_k}{4\pi\varepsilon_0 c^2}\right)^2 {\omega_{aS}}^4 |K(\omega_l)|^2 \frac{\Gamma^R(\omega_{aS})}{\Gamma_0(\omega_{aS})} n_b^{(PSC)}, \tag{80}$$

where the process of radiation is characterized by the corresponding radiative decay rate $\Gamma^R(\omega)$. This decay rate is normalized by the decay rate in the absence of the plasmonic structure, denoted as $\Gamma_0(\omega)$. Both Γ^R and Γ_0 can be obtained from the calculation of the signal emitted by a probe dipolar emitter located at the position of the molecule, and with the same orientation as the Raman dipole induced in the molecule. For an arbitrary environment, $\Gamma^R(\omega)$ and the enhancement $K(\omega)$ can exhibit a complicated frequency dependence.

The radiative decay rate is related to the total decay rate Γ^T (the latter including both radiative and non-radiative channels of decay) and to the radiative yield $\eta(\omega)$. Here we assume a frequency-dependent yield, as we do not limit the discussion to a single Lorentzian mode:

$$\frac{\Gamma^R(\omega)}{\Gamma_0(\omega)} = \frac{\Gamma^T(\omega)}{\Gamma_0(\omega)}\eta(\omega). \tag{81}$$

Furthermore, the total decay rate enhancement is connected with the nanosystem Green's function, $\bar{G}$, as $\Gamma^T(\omega)/\Gamma_0(\omega) = 6\pi(c/\omega)^3 \mathrm{Im}[G_{dd}(\omega)]$. Here Im[ ] indicates the imaginary part and, for simplicity, we have written $G_{dd}(\omega) = \mathbf{u}_d \cdot \bar{G}(\omega, \mathbf{r}_0, \mathbf{r}_0) \cdot \mathbf{u}_d$, where $\mathbf{u}_d$ and $\mathbf{r}_0$ are the orientation and position vectors of the molecular dipole, respectively. Thus, $\mathbf{E}(\mathbf{r}_0,\omega)\cdot\mathbf{u}_d = G_{dd}(\omega)d/\varepsilon_0$ gives the $\mathbf{u}_d$ component of the field excited at position $\mathbf{r}_0$ by a dipole of strength d placed in vacuum at the same position $\mathbf{r}_0$ and with the same orientation $\mathbf{u}_d$.

Inserting eqn (81) into eqn (79) and (80), and using the above relationship between the Green's function and the Purcell factor, we can rewrite the Raman cross-sections in terms of the Green's function of the system as:

$$\sigma_S^{(PSC)} = \frac{\eta(\omega_S)}{c}\left(\frac{Q_k^0 R_k}{\varepsilon_0}\right)^2 \omega_S |K(\omega_l, \mathbf{r}_m)|^2 \times \mathrm{Im}[G_{dd}(\omega_S)]\left(1 + n_b^{(PSC)}\right) \tag{82}$$

and

$$\sigma_{aS}^{(PSC)} = \frac{\eta(\omega_{aS})}{c}\left(\frac{Q_k^0 R_k}{\varepsilon_0}\right)^2 \omega_{aS} |K(\omega_l, \mathbf{r}_m)|^2 \times \mathrm{Im}[G_{dd}(\omega_{aS})] n_b^{(PSC)}. \tag{83}$$

We now assume that the phenomenological classical transition rates, $\Gamma_+^{(PSC)}$ and $\Gamma_-^{(PSC)}$, can still be expressed in terms of these new Raman cross-

sections according to eqn (61). We then obtain the optomechanical transition rates in terms of the Green's function of the system:

$$\Gamma_{+}^{(\mathrm{PSC})} = R_{\mathrm{k}}{}^{2}|K(\omega_{\mathrm{l}}, \mathbf{r}_{\mathrm{m}})|^{2}\mathrm{Im}[G_{\mathrm{dd}}(\omega_{\mathrm{S}})]\frac{|E_0|^2}{4\varepsilon_0\omega_{\mathrm{m}}}, \tag{84}$$

and

$$\Gamma_{-}^{(\mathrm{PSC})} = R_{\mathrm{k}}{}^{2}|K(\omega_{\mathrm{l}}, \mathbf{r}_{\mathrm{m}})|^{2}\mathrm{Im}[G_{\mathrm{dd}}(\omega_{\mathrm{aS}})]\frac{|E_0|^2}{4\varepsilon_0\omega_{\mathrm{m}}}. \tag{85}$$

These transition rates are valid for a general plasmonic environment. Therefore, similarly as we did in Section 2.2, we can write down a master equation for the evolution of the molecular vibrations governed by these transition rates, and immersed in a previously defined thermal bath. With the transition rates $\Gamma_{\pm}^{(\mathrm{PSC})}$ defined above, this master equation exhibits a form very similar to that derived in QMO (eqn (17)) and in PSC (eqn (64)):

$$\begin{aligned}\frac{\mathrm{d}}{\mathrm{d}t}\rho_{\mathrm{b}} = &-\mathrm{i}\left[\omega_{\mathrm{m}}\hat{b}^{\dagger}\hat{b},\ \rho_{\mathrm{b}}\right] + \frac{1}{2}\left[\gamma_{\mathrm{m}}\left(n_{\mathrm{b}}^{\mathrm{th}}+1\right) + \Gamma_{-}^{(\mathrm{PSC})}\right]\mathscr{D}_{\hat{\mathrm{b}}}(\rho_{\mathrm{b}}) \\ &+ \frac{1}{2}\left[\gamma_{\mathrm{m}}n_{\mathrm{b}}^{\mathrm{th}} + \Gamma_{+}^{(\mathrm{PSC})}\right]\mathscr{D}_{\hat{\mathrm{b}}^{\dagger}}(\rho_{\mathrm{b}}),\end{aligned} \tag{86}$$

where we have neglected the small correction originating from the optical spring effect. Finally, we find that by inserting the phenomenological classical transition rates from eqn (84) and (85) into eqn (86), one obtains the same expressions as eqn (19) and (20) in Dezfouli *et al.*[12] We note that Dezfouli *et al.* use an excitation $2E_0\cos(\omega_{\mathrm{l}}t)$ instead of $E_0\cos(\omega_{\mathrm{l}}t)$, which introduces a factor-of-4 difference in the equations.

D Table of symbols

γ_{m}	Phonon decay rate
κ	Plasmon decay rate
ω_{m}	Phonon resonance frequency
ω_{c}	Plasmon resonance frequency
ω_{l}	Laser frequency
$n_{\mathrm{b}}^{\mathrm{th}}$	Thermal phonon population
V	Effective plasmon mode volume
α_{L}	Molecular polarizability
Q_{k}	Normal mode coordinate
Q_{k}^{0}	Zero-point amplitude
R_{k}	Raman tensor element
$\hat{a}$, $\hat{a}^{\dagger}$	Annihilation and creation plasmon operators
$\hat{b}$, $\hat{b}^{\dagger}$	Annihilation and creation phonon operators
g_0	Single-plasmon optomechanical coupling rate
Ω	Coherent pumping rate
$\Delta = \omega_{\mathrm{c}} - \omega_{\mathrm{l}}$	Cavity-laser detuning
α	Coherent plasmon amplitude (QMO)
$\delta\hat{a}$	Plasmon fluctuations operator
β	Coherent phonon amplitude (QMO)

$\delta\hat{b}$	Phonon fluctuations operator (QMO)
$n_{\delta b}$	Incoherent phonon population (QMO)
n_b	Phonon population (QMO)
Γ_+	Enhancement of phonon creation rate (QMO)
Γ_-	Enhancement of phonon annihilation rate (QMO)
Γ_{opt}	Optomechanical damping
ω_S (ω_{aS})	Stokes (anti-Stokes) emission frequency
$\alpha^{(CMO)}$	Coherent plasmon amplitude (CMO)
$n_b^{(CMO)}$	Phonon population (CMO)
σ_S^0 (σ_{aS}^0)	Stokes (anti-Stokes) cross sections
$\sigma_S^{(PSC)}$	Plasmon-enhanced Stokes cross sections
$\sigma_{aS}^{(PSC)}$	Plasmon-enhanced anti-Stokes cross sections
L_m	Electromagnetic local field correction
$n_b^{(PSC)}$	Phonon population (PSC)
$K(\omega)$	Plasmonic field enhancement
$n_b^{(vp)}$	Vibrationally pumped phonon population (PSC)
$n_b^{(vp)}\|_{low\ I}$	Vibrationally pumped phonon population (PSC) for low illumination intensity
$n_{\delta b}^{(vp)}$	Vibrationally pumped phonon population (QMO)
$n_{\delta b}^{(vp)}\|_{low\ I}$	Vibrationally pumped phonon population (QMO) for low illumination intensity
$\Gamma_+^{(PSC)}$	Enhancement of phonon creation rate (PSC)
$\Gamma_-^{(PSC)}$	Enhancement of phonon annihilation rate (PSC)

Acknowledgements

The authors would like to thank Christophe Galland, Geza Giedke, Alejandro González-Tudela, Eric Le Ru, Mathieu Juan and Andreas Nunnenkamp for stimulating discussions. MKS, RE and JA acknowledge support from MINECO project FIS2016-80174-P, NIST grant 70NANB15H32 of the Department of Commerce of the US, and the COST Action MP1403 "Nanoscale Quantum Optics" supported by COST (European Cooperation in Science and Technology). FB and JJB acknowledge financial support from EPSRC grants EP/G060649/1, EP/K028510/1, EP/L027151/1, EP/G037221/1, EPSRC NanoDTC EP/L015978/1, and ERC grant LINASS 320503. F. B. acknowledges support from the Winton Programme for the Physics of Sustainability.

References

1 H. Xu, J. Aizpurua, M. Käll and P. Apell, *Phys. Rev. E: Stat. Phys., Plasmas, Fluids, Relat. Interdiscip. Top.*, 2000, **62**, 4318.
2 M. Moskovits, *J. Raman Spectrosc.*, 2005, **36**, 485–496.
3 C. Ciracì, R. Hill, J. Mock, Y. Urzhumov, A. Fernández-Domínguez, S. Maier, J. Pendry, A. Chilkoti and D. Smith, *Science*, 2012, **337**, 1072–1074.
4 L. Tong, H. Xu and M. Käll, *MRS Bull.*, 2014, **39**, 163–168.
5 D. N. Klyshko, *Quantum Electron.*, 1977, **7**, 755.
6 C. A. Parra-Murillo, M. F. Santos, C. H. Monken and A. Jorio, *Phys. Rev. B*, 2016, **93**, 125141.

7 A. Jorio, M. Kasperczyk, N. Clark, E. Neu, P. Maletinsky, A. Vijayaraghavan and L. Novotny, *Nano Lett.*, 2014, **14**, 5687–5692.
8 K. Kneipp, Y. Wang, H. Kneipp, L. T. Perelman, I. Itzkan, R. R. Dasari and M. S. Feld, *Phys. Rev. Lett.*, 1997, **78**, 1667.
9 P. Roelli, C. Galland, N. Piro and T. J. Kippenberg, *Nat. Nanotechnol.*, 2015, **11**, 164–169.
10 M. K. Schmidt, R. Esteban, A. González-Tudela, G. Giedke and J. Aizpurua, *ACS Nano*, 2016, **10**, 6291–6298.
11 M. Aspelmeyer, T. J. Kippenberg and F. Marquardt, *Rev. Mod. Phys.*, 2014, **86**, 1391–1452.
12 M. K. Dezfouli and S. Hughes, *ACS Photonics*, 2017, **4**, 1245–1256.
13 F. Benz, M. K. Schmidt, A. Dreismann, R. Chikkaraddy, Y. Zhang, A. Demetriadou, C. Carnegie, H. Ohadi, B. de Nijs, R. Esteban, J. Aizpurua and J. J. Baumberg, *Science*, 2016, **354**, 726–729.
14 L. Novotny and B. Hecht, *Principles of Nano-Optics*, Cambridge University Press, Cambridge, England, 2006.
15 R. Esteban, J. Aizpurua and G. W. Bryant, *New J. Phys.*, 2014, **16**, 013052.
16 E. Waks and D. Sridharan, *Phys. Rev. A*, 2010, **82**, 043845.
17 E. C. L. Ru and P. G. Etchegoin, *Principles of Surface-Enhanced Raman Spectroscopy*, Elsevier, Amsterdam, 2009.
18 A. Merlen, J. Valmalette, P. Gucciardi, M. Lamy de La Chapelle, A. Frigout and R. Ossikovski, *J. Raman Spectrosc.*, 2009, **40**, 1361–1370.
19 D. Bougeard and K. S. Smirnov, *J. Raman Spectrosc.*, 2009, **40**, 1704–1719.
20 V. Gorini, A. Kossakowski and E. C. G. Sudarshan, *J. Math. Phys.*, 1976, **17**, 821–825.
21 G. Lindblad, *Commun. Math. Phys.*, 1976, **48**, 119–130.
22 I. Wilson-Rae, N. Nooshi, W. Zwerger and T. J. Kippenberg, *Phys. Rev. Lett.*, 2007, **99**, 093901.
23 F. Marquardt, J. P. Chen, A. A. Clerk and S. M. Girvin, *Phys. Rev. Lett.*, 2007, **99**, 093902.
24 P. Degenfeld-Schonburg, M. Abdi, M. J. Hartmann and C. Navarrete-Benlloch, *Phys. Rev. A*, 2016, **93**, 023819.
25 I. Wilson-Rae, N. Nooshi, J. Dobrindt, T. J. Kippenberg and W. Zwerger, *New J. Phys.*, 2008, **10**, 095007.
26 M. Aspelmeyer, T. J. Kippenberg and F. Marquardt, *Cavity optomechanics: nano- and micromechanical resonators interacting with light*, Springer, 2014.
27 M. Benito, C. Sánchez Muñoz and C. Navarrete-Benlloch, *Phys. Rev. A*, 2016, **93**, 023846.
28 A. Lombardi, L. Weller, F. Benz, M. K. Schmidt, B. de Nijs, J. Aizpurua and J. J. Baumberg, submitted.
29 E. A. Pozzi, A. B. Zrimsek, C. M. Lethiec, G. C. Schatz, M. C. Hersam and R. P. Van Duyne, *J. Phys. Chem. C*, 2015, **119**, 21116–21124.
30 E. C. Le Ru and P. G. Etchegoin, *Faraday Discuss.*, 2006, **132**, 63–75.
31 R. Maher, P. Etchegoin, E. Le Ru and L. Cohen, *J. Phys. Chem. B*, 2006, **110**, 11757–11760.
32 E. A. Pozzi, N. L. Gruenke, N. Chiang, D. V. Zhdanov, N. Jiang, T. Seideman, G. C. Schatz, M. C. Hersam and R. P. Van Duyne, *J. Phys. Chem. Lett.*, 2016, **7**, 2971–2976.

33 R. C. Maher, L. F. Cohen, J. C. Gallop, E. C. Le Ru and P. G. Etchegoin, *J. Phys. Chem. B*, 2006, **110**, 6797–6803.
34 M. Baibarac, I. Baltog, L. Mihut, A. Matea and S. Lefrant, *J. Opt.*, 2014, **16**, 035003.
35 P. Zolotavin, A. Alabastri, P. Nordlander and D. Natelson, *ACS Nano*, 2016, **10**, 6972–6979.
36 L. Khosravi Khorashad, L. V. Besteiro, Z. Wang, J. Valentine and A. O. Govorov, *J. Phys. Chem. C*, 2016, **120**, 13215–13226.
37 M. Moskovits, *Rev. Mod. Phys.*, 1985, **57**, 783.
38 R. W. Taylor, T.-C. Lee, O. A. Scherman, R. Esteban, J. Aizpurua, F. M. Huang, J. J. Baumberg and S. Mahajan, *ACS Nano*, 2011, **5**, 3878–3887.
39 S. T. Jones, R. W. Taylor, R. Esteban, E. K. Abo-Hamed, P. H. Bomans, N. A. Sommerdijk, J. Aizpurua, J. J. Baumberg and O. A. Scherman, *Small*, 2014, **10**, 4298–4303.
40 R. Carminati, J. J. Sáenz, J.-J. Greffet and M. Nieto-Vesperinas, *Phys. Rev. A*, 2000, **62**, 012712.
41 C. M. Galloway, P. G. Etchegoin and E. C. Le Ru, *Phys. Rev. Lett.*, 2009, **103**, 063003.
42 C. Galloway, E. Le Ru and P. Etchegoin, *Phys. Chem. Chem. Phys.*, 2009, **11**, 7372–7380.
43 K. Kneipp, Y. Wang, H. Kneipp, I. Itzkan, R. R. Dasari and M. S. Feld, *Phys. Rev. Lett.*, 1996, **76**, 2444–2447.
44 P. Rabl, *Phys. Rev. Lett.*, 2011, **107**, 063601.
45 A. Nunnenkamp, K. Børkje and S. M. Girvin, *Phys. Rev. Lett.*, 2011, **107**, 063602.
46 M. K. Schmidt, R. Esteban, G. Giedke, J. Aizpurua and A. González-Tudela, in preparation.
47 A. González-Tudela, D. Martin-Cano, E. Moreno, L. Martin-Moreno, C. Tejedor and F. J. Garcia-Vidal, *Phys. Rev. Lett.*, 2011, **106**, 020501.
48 R. Beams, L. G. Cançado, S.-H. Oh, A. Jorio and L. Novotny, *Phys. Rev. Lett.*, 2014, **113**, 186101.
49 L. G. Cançado, R. Beams, A. Jorio and L. Novotny, *Phys. Rev. X*, 2014, **4**, 031054.
50 W. Zhu and K. B. Crozier, *Nat. Commun.*, 2014, **5**, 5228.
51 M. Barbry, P. Koval, F. Marchesin, R. Esteban, A. G. Borisov, J. Aizpurua and D. Sánchez-Portal, *Nano Lett.*, 2015, **15**, 3410–3419.
52 P. Zhang, J. Feist, A. Rubio, P. García-González and F. J. García-Vidal, *Phys. Rev. B: Condens. Matter Mater. Phys.*, 2014, **90**, 161407.